Toxicology in Vitro 48 (2018) 205–220

Contents lists available at ScienceDirect

Toxicology in Vitro

journal homepage: www.elsevier.com/locate/toxinvit

Azilsartan and its Zn(II) complex. Synthesis, anticancer mechanisms of action and binding to bovine serum albumin

Valeria R. Martínez[a], María V. Aguirre[b], Juan S. Todaro[b], Oscar E. Piro[c], Gustavo A. Echeverría[c], Evelina G. Ferrer[a], Patricia A.M. Williams[a,*]

[a] Centro de Química Inorgánica (CEQUINOR-CONICET-UNLP), 120 N° 1465, La Plata, Argentina
[b] Laboratorio de Investigaciones Bioquímicas, Facultad de Medicina, UNNE, Moreno 1240, Corrientes, Argentina
[c] Departamento de Física, Facultad de Ciencias Exactas, Universidad Nacional de La Plata y IFLP (CONICET, CCT La Plata), C.C. 67, 1900 La Plata, Argentina

ARTICLE INFO

Keywords:
Azilsartan
Zn(II)-Azilsartan complex
Anticancer mechanisms
BSA interactions

ABSTRACT

Azilsartan is the eighth approved member of angiotensin II receptor blockers for hypertension treatment. Considering that some drugs have additional effects when administered, we studied its effects and mechanisms of action on a human lung cancer cell line A549. We have also modified the structure of the drug by complexation with Zn(II) cation and assayed the anticancer effect. The crystal structure of the new binuclear Zn(II) complex, for short $[Zn_2(azil)_2(H_2O)_4]\cdot 2H_2O$ (ZnAzil), was determined by X-ray diffraction methods. The zinc ions are bridged by azilsartan ligands through their carboxylate oxygen and oxadiazol nitrogen atoms. The compounds were examined for their cytotoxic effects against human lung fibroblast (MRC5) and human lung cancer (A549) cell lines. Azilsartan displayed low cytotoxic effects at 150 μM concentrations in A549 human lung cancer cells but the higher effect measured for the Zn complex suggested that this compound may act as an anticancer agent. An apoptotic oxidative stress mechanism of action via the mitochondrial-dependent intrinsic pathway has been determined. Besides, the compounds exerted weak cytotoxic effects in the normal lung related cell line MRC5. Binding constants of the complex formed between each compound and bovine serum albumin (BSA) are in the intermediate range, hence suggesting that azilsartan and ZnAzil could be bonded and transported by BSA.

1. Introduction

Hypertension affects approximately one in three adults in the world and is a major risk factor for cardiovascular disease. One of the eight classes of medications used in the treatment of hypertension are the angiotensin II (Ang II) receptor blockers (ARBs). Azilsartan is the eighth ARB to be approved for the treatment of hypertension and received FDA approval in February 2011 (Zaiken and Cheng, 2011). Azilsartan medoxomil (postassium salt) is the prodrug that undergoes rapid hydrolysis to liberate azilsartan, the active ingredient (Ding et al., 2013). Azilsartan is structurally similar to candesartan, another ~~other~~ antihypertensive pharmaceutical, in which the tetrazole ring has been replaced by a 5-oxo-1,2,4-oxadiazole (Fig. 1). This group is related to the stronger molecular mode of binding to the angiotensin II type 1 receptor (AT1R) and slow dissociation from the receptor, which gave the drug the superior efficacy to lower blood pressure (Tamura et al., 2013). It has been reported that the AT1R has been found in several kind of cancer cells and that Ang II would be involved in tumor angiogenesis (Goldfarb et al., 1994). In fact, AT1R have been found in the human lung cancer cell line A549 (Batra et al., 1994). Ang II can induce neovascularization in experimental systems due to the expression of different growth factors such as angiopoietin 2, vascular endothelial factor, and its receptor (Escobar et al., 2004) and this is an essential process for the growth and metastasis of solid cancerous tumors (Weidner et al., 1991). Besides, ATR1 is overexpressed in ovary, bladder, lung, and breast cancers (Oh et al., 2015) and the inhibition of angiogenesis, growth, and metastasis of tumors is highly dependent on AT1R blockade (Mamoru et al., 2002).

Abbreviations: 4CN, 4-chloro-1-naphthol; Ang II, angiotensin II; AO, acridine orange; ARBs, angiotensin receptor blockers; Azil, azilsartan; Bax, Bcl-2-associated X protein; Bcl-xL, B-cell lymphoma-extra large; BSA, bovine serum albumin; DCF, 2′,7′-dichlorofluorescein; DMEM, Dulbeco's modified Eagle's Medium; DMSO, dimethyl sulfoxide; EDTA, ethylenediaminetetraacetic acid; EGTA, ethylene glycol-bis(β-aminoethyl ether)-*N*,*N*,*N*′,*N*′-tetraacetic acid; EtBr, ethidium bromide; FBS, fetal bovine serum; GSH, reduced glutathione; GSSG, oxidized glutathione; H2DCFDA, 2′,7′-dichlorodihydrofluorescein diacetate; MTT, 3-(4,5-dimethylthiazol-2-yl)-2,5-diphenyltetrazolium bromide; NAC, *N*-acetylcysteine; NEM, *N*-ethyl maleimide; OPT, *o*-phthalaldehyde; PAGE, polyacrylamide gel electrophoresis; PBS, phosphate buffered saline; PMSF, phenylmethylsulfonyl fluoride; RIPA buffer, radioimmunoprecipitation assay buffer; ROS, reactive oxygen species; SDS, dodecyl sulfate; Zincon, 2-[2-[(Z)-*N*-[(*E*)-(6-oxo-3-sulfocyclohexa-2,4-dien-1-ylidene)amino]-C-phenylcarbonimidoyl]hydrazinyl]benzoic acid; ZnAzil, $[Zn_2(azil)_2(H_2O)_4]\cdot 2H_2O$

* Corresponding author.
E-mail address: williams@quimica.unlp.edu.ar (P.A.M. Williams).

https://doi.org/10.1016/j.tiv.2018.01.009
Received 24 October 2017; Received in revised form 15 December 2017; Accepted 14 January 2018
0887-2333/ © 2018 Elsevier Ltd. All rights reserved.

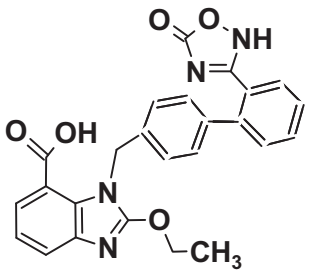

Fig. 1. Schematic structure of azilsartan.

Metal ions play a crucial role in biological systems. Coordination complexes used in medicine with a wide variety of geometries and reactivities are currently an area of intense research in bioinorganic chemistry. It is well known that the biometal-drug complexation modulates the pharmacological actions of therapeutic ligands due to a synergistic effect. (Gaberc-Porekar et al., 2011; Ndagi et al., 2017; Frezza et al., 2010). In particular, Zn(II), an essential trace element constituent of proteins, hormones, peptides and receptors is involved in many important physiological processes, including metabolism, signaling, proliferation, gene expression and apoptosis. Zn(II) ion also has antioxidant properties and it has been shown that its deprivation in diet increases the cellular susceptibility to oxidative stress. For this reason, certain diseases are associated with Zn(II) deficiency, including hypertension (Jurowski et al., 2014). Besides, zinc oxide has been used in the form of topical creams in the treatment of various skin conditions (e.g. diaper rash) (Šikić Pogačar et al., 2017; Bookout et al., 2004). Likewise, its deficiency is associated with cancer. Supplementation with this biometal in the diet has managed to lower tumor risk since it reduces oxidative stress and improves immune function (Ho, 2004). Besides, it has been reported that exogenous zinc stress produces toxic effects in cancer cell lines. Lung cancer A549 cells response to zinc stress and the MTT assay and flow cytometric analysis showed that the $ZnSO_4$ treatment led to a bi-phasic variation in viability and a slight fluctuation in the apoptosis of A549 cells (Yuan et al., 2012).

In addition, the in vitro cell system for the appropriate cell types is a good laboratory model to investigate the biochemistry and possible mechanisms of action employed by the metal complex to exert its actions. One major challenge in anticancer therapy is to increase the selectivity of current treatments toward cancer cells. The anticancer agents must exert minimal adverse effects on normal tissues with maximal capacity to kill tumor cells and/or inhibit tumor growth. On the other side, it is well known that serum albumin is a transporter for different types of endogenous and exogenous compounds such as drugs, fatty acids and dyes in the bloodstream. The binding of this protein to small molecules such as drugs can significantly affect their absorption, distribution, metabolism and toxicity. It is also well established that numerous small-molecule compounds are capable of binding various target proteins and exhibit their antitumor activity (Zhang et al., 2016) improving their effects in some cases.

Hence, it could be interesting to design a metal coordination complex by the combination of azilsartan with Zn(II) ions, and examine its effectiveness as a potential anticancer agent. Herein, we report the syntheses and characterization of tetraaquobis(μ-2-ethoxy-3-[[4-[2-(5-oxo-1,2,4-oxadiazol-3-yl)phenyl]phenyl]methyl] benzimidazole-4-carboxylate-*N*-,*O*-) dizinc(II) dihydrate and its in vitro cytotoxicity and the determination of the possible mechanisms of action against some cancer cells. With comparative purposes, the biological effects of azilsartan were also evaluated. We find that the metal complex showed anticancer action on the A549 cancer cell line generating a synergistic effect in comparison with azilsartan. Our studies showed that the possible mechanisms of action involved reactive oxygen species (ROS) generation and cellular antioxidant status depletion. Additionally, to evaluate the possibility that both compounds could be transported in the bloodstream, the binding affinity of azilsartan and ZnAzil with the serum albumin has been studied.

2. Materials and methods

2.1. Experimental

Azilsartan was purchased from Rundu Pharma (Shangai, China) and Zinc (II) chloride from Biopack, Argentina (97% purity) and used as supplied. A sodium silicate solution (14% NaOH-27% SiO_2, SiO_2.NaOH, Sigma-Aldrich) was used for the gel diffusion method. All other chemicals were of analytical grade and used without further purification. Infrared spectra of powdered samples were measured with a Bruker IFS 66 FTIR-spectrophotometer from 4000 to 400 cm^{-1} using the KBr pellet technique. Elemental analyses for carbon, hydrogen and nitrogen were performed using a Carlo Erba EA 1108 analyzer. Zn content was determined with Zincon (2-[2-[(Z)-*N*-[(*E*)-(6-oxo-3-sulfocyclohexa-2,4-dien-1-ylidene)amino]-C-phenylcarbonimidoyl]hydrazinyl]benzoic acid). A stock solution of Zincon sodium salt (1.6 mM, 0.007 g, Santa Cruz Biotechnology) was prepared by mixing the powder with 200 μL NaOH 1 M and reaching a final volume of 10 mL with distilled water. Different concentrations of ZnAzil and $ZnSO_4$ (25 μL) in the 0–40 μM range were dissolved in 950 μL borate buffer (final concentration: 50 mM, pH 9.0) and 25 μL of Zincon stock solution. Following incubation at 20 °C for 5 min, the absorbance at 620 nm was recorded. The relationship between the metal and the complex was calculated from the respective $ZnSO_4$ calibration curve (Säbel et al., 2010). Thermogravimetric analysis (TG) and differential thermal analysis (DTA) were measured with a Shimadzu system (model TG-50), working under oxygen flow of 50 mL/min and at a heating rate of 10 °C/min. Sample quantities ranged between 5 and 10 mg. Electronic absorption spectra were recorded on a Hewlett-Packard 8453 diode-array spectrophotometer, using 1 cm quartz cells. Fluorescence spectra were measured using a Shimadzu RF-6000 spectrophotometer.

2.2. Preparation of $[Zn_2(azil)_2(H_2O)_4]\cdot 2H_2O$

Azilsartan (0.1 mmol, 0.0456 g) was dissolved in methanol (10 mL) and then $ZnCl_2$ (0.1 mmol, 0.0136 g) in methanol (5 mL) was added to give a clear solution that was stirred during 10 min. The reaction mixture precipitated after two days. The solid was filtered out, washed with cold methanol and dried in an oven at 60 °C. Elemental analysis (%): Calcd. for $C_{50}H_{48}N_8O_{16}Zn_2$: C, 52.3; H, 4.2; N, 9.8; Zn, 11.4. Found: C, 52.5; H, 4.2; N, 9.7; Zn, 11.3.

UV–vis spectrum (1×10^{-5} M, DMSO): ZnAzil, λ_m 284 nm; $\varepsilon = 1.02 \times 10^4\ M^{-1}\ cm^{-1}$; azilsartan, λ_m 281 nm, $\varepsilon = 9.70 \times 10^3\ M^{-1}\ cm^{-1}$. Thermogravimetric (TG) and differential thermogravimetric analysis (DTA) were carried out for the complex under oxygen flow. The TG curve showed that the complex started to lose weight at 30 °C with the loss of 6 water molecules up to 155 °C ($\Delta\omega_{exp}$ = 9.3% and $\Delta\omega_{calc}$ = 9.4%, DTA, *endo* 60 °C and 115 °C, very broad). The decomposition continues to about 450 °C at which point most of the organic part of the compounds have been lost (DTA 440 °C *exo*, very strong). The final residue at 800 °C of 14.3% is in agreement with the calculated residue (14.2%) considering ZnO as the decomposition products. The presence of ZnO in the residue has been confirmed by FTIR spectroscopy. Colorless crystals suitable for X-ray determinations were obtained using the gel three layer technique. Sodium silicate was dissolved in water (5% v/v) and the pH value was adjusted to 7 using 50% HCl (solution A). A bottom gel layer (15 mL) of solution A mixed with a methanolic solution of azilsartan (0.0228 g) was placed in a 25 × 200 mm glass tube. After gelification, the middle layer of 15 mL solution A and the top layer (15 mL) of solution A with a methanolic solution of $ZnCl_2$ (0.068 g mL) were added. Single crystals of ZnAzil were grown after two months. Both the crystal and the powder samples showed the same vibration spectral pattern (see below) then, it

has been inferred that they share the same structure.

2.3. Single crystal X-ray diffraction data

The measurements were performed on an Oxford Xcalibur Gemini, Eos CCD diffractometer with graphite-monochromated MoKα (λ = 0.71073 Å) radiation. X-ray diffraction intensities were collected (ω scans with ϑ and κ-offsets), integrated and scaled with CrysAlisPro suite of programs (CrysAlisPro, 2009). The unit cell parameters were obtained by least-squares refinement (based on the angular settings for all collected reflections with intensities larger than seven times the standard deviation of measurement errors) using CrysAlisPro. Data were corrected empirically for absorption employing the multi-scan method implemented in CrysAlisPro. The structure was solved by the intrinsic phasing method implemented in SHELXT of the SHELX suit of programs (Sheldrick, 2008) and refined by full-matrix least-squares with SHELXL of the same package. All but the water hydrogen atoms were positioned on stereo-chemical basis and refined with the riding model. The methyl H-atoms were refined as rigid group allowed to rotate around the C—CH_3 bond such as to maximize the sum of the residual density at the calculated positions. The methyl group converged to a staggered rotational conformation. The H-atoms of the two coordination water molecules were located in a difference Fourier map and refined at their found positions with isotropic displacement parameters and O—H and H…H distances restrained to target values of 0.86(1) and 1.36(1) Å. The crystallization water H-atoms could not be located reliably in the final residual electron density map and therefore they are not included in the final molecular model.

2.4. Antitumor activity evaluation

2.4.1. Cell culture and viability assays

The human lung fibroblast cell line (MRC5) and the human lung cancer cell lines (A549) were cultured in Dulbeco's modified Eagle's Medium (DMEM) supplemented with 5% (v/v) fetal bovine serum (FBS), 100 U/mL penicillin-streptomycin, at 37 °C in a humidified incubator with 5% CO_2. Cells were harvested at 85% confluence using PBS-EDTA and then suspended at a final concentration of 2×10^6 cells/mL into 6-well plates, 48-well plates, 35 mm dishes, according to the selected experiment. To examine the effect of the compounds, cells were treated with the compounds at different concentrations and then they were assessed in three independent experiments.

For the viability assays, the A549 carcinoma cells were cultured in 48-well plates. After 24 h of incubation, cells were exposed to different concentrations of $ZnSO_4$, azilsartan and ZnAzil (0, 2.5, 5, 10, 25, 50, 75, 100 and 250 μM). Then, cell viability was determined through the 3-(4,5-dimethylthiazol-2-yl)-2,5-diphenyltetrazolium bromide (MTT) assay (Glaysher and Cree, 2011). A volume of 250 μL of MTT solution was added to each well in an amount equal to 10% of culture volume and cells were incubated for 1.5 h at 37 °C until a purple-colored formazan product developed. The formazan precipitate was dissolved in acidified isopropanol under vigorously stirred. The absorbance at 560 nm was measured by UV–VIS spectroscopy.

2.4.2. Reactive oxygen species assay

Intracellular reactive oxygen species (ROS) generated by the compounds was evaluated using 2′,7′-dichlorodihydrofluorescein diacetate (H2DCFDA) by a fluorometric quantitative assay (Ling et al., 2011). Treated cells with $ZnSO_4$, azilsartan and ZnAzil (0–250 μM) were incubated in 10 μM H2DCFDA solution for 30 min at 37 °C under light protection. Lysate cells were measured at 485 nm excitation and 528 nm emission wavelengths. Results were presented as the percentage of fluorescence intensity relative to the basal measurements ± standard error.

Using the same assay as described above, ROS generation in the A549 cell line was measured in the presence of NAC (*N*-acetylcysteine). Cells were pretreated with 5 mM of NAC for 30 min, followed by treatment with the compounds at different concentrations for additional 24 h.

2.4.3. Estimation of cell glutathione (GSH) and oxidized glutathione (GSSG) content

A modification of Hissin and Hilf's method was used for the determination of reduced (GSH) and oxidized glutathione (GSSG) content in treated A549 cells (Hissin and Hilf, 1976). Protein contents in each cellular extract were quantified using the Bradford method (Bradford, 1976). Standard concentrations of GSH and GSSG (0.05–1.0 μg/mL) were used. The fluorescence spectra were recorded at 350 nm excitation and 420 nm emission wavelengths. The concentrations in μg GSH/mg protein were calculated from the respective calibration curves. The ratio GSH/GSSG was expressed as a percentage of the basal for all the experimental conditions.

2.4.4. Apoptosis and necrosis assay; cell morphology

Acridine orange/ethidium bromide (AO/EtBr) staining was carried out to detect morphological evidence of apoptosis and necrosis (Martin and Leonardo, 1998). Briefly, cells treated with $ZnSO_4$, azilsartan and ZnAzil (155 μM) for 24 h were stained with 4 μg/mL acridine orange and 4 μg/mL ethidium bromide and were immediately examined under a fluorescence microscope (Olympus CX-35) at 10× and 40× magnification. Viable (normal, green nuclei), apoptotic (condensed, orange nuclei) and necrotic (normal, red nuclei) cells were counted. 200 cells per slide were analyzed in each of three independent experiments.

2.4.5. Western blot analysis

Bax, Bcl-xL and caspase-9 expression were determined by immunoblotting analysis (Aguirre et al., 2005). A549 cell cultures were incubated with $ZnSO_4$, azilsartan and ZnAzil (155 μM, IC_{50} value for the complex) for 24 h. Protein content in lysates was determined by the Bradford method. Proteins were resolved by SDS-PAGE and transferred to a nitrocellulose membrane (BioRad, CA, USA). Membranes were blocked and then were incubated overnight at 4 °C with the following primary antibodies: anti-Bax (1:750), anti-Bcl-xL (1:1000) and Caspase-9 (1:750) (Santa Cruz Biotechnology, Santa Cruz, CA, USA) or anti-β actin (Sigma-Aldrich). The technique was followed with incubation for 1 h at room temperature with horseradish peroxidase-conjugated secondary antibodies (Jackson Immunoresearch Inc., USA). β-Actin detection was used to normalize immunoblottings. Immunocomplexes were detected by an Opti4CN kit (Bio-Rad, CA, USA). Band optical density (OD) was analyzed using Scion-beta 2 image software and results were expressed as the ratio (protein of interest OD/β-actin OD) ×100. All experiments have been performed by triplicate and two representative immunoreactive bands of one experiment and each sample are shown.

2.5. Bovine serum albumin (BSA) interaction

BSA was dissolved in Tris-HCl (0.1 M, pH 7.4) buffer to attain a final concentration of 6 μM. The albumin concentration is usual for fluorescence quenching experiments. Azilsartan and ZnAzil were added dropwise to the BSA solution and left to rest to ensure the formation of homogeneous solutions with concentrations ranging from 2 to 20 μM. Each solution was mixed fully and incubated at 25, 30 and 37 °C for 1 h. The fluorescence spectra were measured at 280 nm excitation and the spectral bandwidths of excitation and emission slit were both set at 10 nm. The measurements were carried out on Shimadzu RF-6000 spectrofluorometer. Curve-fitting method with the Levenberg–Marquadt algorithm has been used to deconvolute the fluorescence bands and the peaks corresponding to BSA (λ_{max}: 336 nm) and azilsartan or ZnAzil (λ_{max}: 368 nm for both compounds) were adjusted. Base line corrections, normalization, curve-fitting and calculations were performed by OriginPro 9.1.0 (OriginLab Corporation,

Table 1
Crystal data and structure refinement results for $[Zn_2(azil)_2(H_2O)_4]\cdot 2H_2O$.

Empirical formula	$C_{50}H_{48}N_8O_{16}Zn_2$
Formula weight	1147.70
Temperature	293(2) K
Wavelength	0.71073 Å
Crystal system	Monoclinic
Space group	$P\ 2_1/n$
Unit cell dimensions	a = 15.038(1) Å b = 10.8207(4) Å c = 16.8623(9) Å β = 103.192(7)°
Volume	2671.4(3) Å^3
Z, density (calculated)	2, 1.427 Mg/m^3
Absorption coefficient	0.973 mm^{-1}
F(000)	1184
Crystal size	0.297 × 0.073 × 0.033 mm^3
ϑ-range for data collection	3.172 to 29.036°
Index ranges	$-19 \le h \le 20,\ -12 \le k \le 14,\ -12 < l \le 22$
Reflections collected	13,103
Independent reflections	5916 [R(int) = 0.0883]
Completeness to ϑ = 25.242°	99.8%
Observed reflections [I > 2σ(I)]	2894
Refinement method	Full-matrix least-squares on F^2
Data/restraints/parameters	5916/6/360
Goodness-of-fit on F^2	1.019
Final R indices[a] [I > 2σ(I)]	$R1$ = 0.0810, wR2 = 0.1998
R indices (all data)	$R1$ = 0.1803, wR2 = 0.2503
Largest diff. Peak and hole	1.671 and −0.434 e·Å^{-3}

[a] $R_1 = \Sigma||F_o| - |F_c|| / \Sigma|F_o|$, $wR_2 = [\Sigma w(|F_o|^2 - |F_c|^2)^2 / \Sigma w(|F_o|^2)^2]^{1/2}$.

Northampton, USA) software.

2.6. Statistical analysis

Data are expressed as the mean ± standard error (SE). The Sigma plot software package was used for statistical analysis. An analysis of variance (One way ANOVA) was applied to compare the means of multiple groups of measured data. Significance was defined as $P < 0.05$.

3. Results and discussion

3.1. Crystallographic structural results and discussion

Crystal data, data collection procedure, structure determination methods and refinement results are summarized in Table 1.

As shown in the ORTEP (Farrugia, 1997) drawing of Fig. 2, the solid state molecule is arranged as a centre-symmetric Zn(II) binuclear complex. Bond distances and angles around Zn(II) ion are detailed in Table 2. The azilsartan ligand is negatively double-charged by loss of the protons at the terminal carboxylate and oxadiazol groups. The metal is in a distorted tetrahedral $ZnON(Ow)_2$ environment, coordinated to one carboxylic O-atom of an azilsartan ligand [d(Zn—O) = 1.942(4) Å], to the pyridine-like N-atom of the oxadiazol of another, inversion related, ligand [d(Zn—N) = 1.989(5) Å] and to two water molecules [Cd—Ow bond distances of 1.974(6) and 1.948(5) Å]. L—Zn—L bond angles are in the range from 99.6(2) to 128.6(2)°.

Observed bond distances and angles within azilsartan anion agree with corresponding metrics reported for the solid state neutral azilsartan (Ge et al., 2016). As expected the major differences occur in bond lengths affected by the above mentioned double deprotonation and the binding to the metal. In fact, at the carboxylic end C=O and C—OH bonding distances of 1.222(4) and 1.308(4) Å in the neutral pharmaceutical are now 1.224(8) and 1.277(8) Å in the coordinated-to-metal charged ligand of $[Zn_2(azil)_2(H_2O)_2]$ complex, while at the oxadiazol end, N—C bond lengths involving the coordinated-to-metal N-atom which are 1.359(5) and 1.369(4) Å for neutral azilsartan are now equal to 1.356(8) and 1.357(8) Å in the zinc complex.

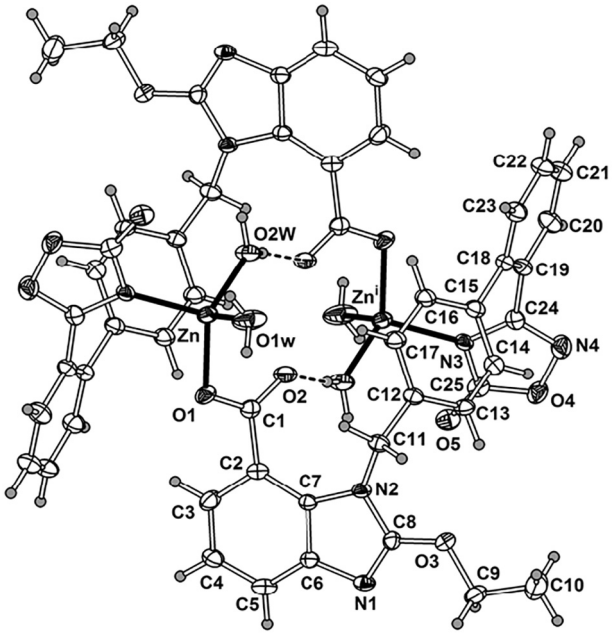

Fig. 2. Drawing of solid state binuclear $[Zn_2(azil)_2(H_2O)_4]$ complex showing the labeling of the non-H atoms and their displacement ellipsoids at the 30% probability level. Zinc-ligand bonds are indicated by full lines and intra-molecular H-bonds by dashed lines. Except for the metal, only the atoms of the independent half molecule have been labeled. The other half is the centre-symmetric counterpart generated by the inversion symmetry operation (i): 1 − x, 1 − y, 1 − z.

Table 2
Bond lengths [Å] and angles [°] around Zn(II) ion in $[Zn_2(azil)_2(H_2O)_4]\cdot 2H_2O$.

Zn—O(1)	1.942(4)	O(1)—Zn—O(2W)	128.6(2)
Zn—N(3′)	1.989(5)	O(1)—Zn—O(1W)	99.6(2)
Zn—O(1W)	1.974(6)	O(2W)—Zn—O(1W)	101.7(3)
Zn—O(2W)	1.948(5)	O(1)—Zn—N(3′)	105.5(2)
		O(2W)—Zn—N(3′)	109.7(2)
		O(1W)—Zn—N(3′)	110.6(3)

Primed N(3) atom is related to the unprimed one by the inversion symmetry operation: −x + 1, −y + 1, −z + 1.

The binuclear complex is further stabilized by an intra-molecular OwH…O bond involving as acceptor the other carboxylic O-atom [d(Ow…O) = 2.726(8) A, ∠(Ow—H…O) = 169(10)°]. H-bonding structure is further detailed in Table 3.

3.2. Vibrational spectroscopy

Both the single crystal and the powder complex displayed the same spectral infrared pattern, denoting that they have the same structures. The assignments have been performed by comparison with the reported vibration spectra of the structurally related sartan, candesartan (Islas et al., 2012) and that of the 5-oxo-1,2,4-oxadiazole group (Hemming, 2008). The most characteristic FTIR bands of the ligand and the

Table 3
Hydrogen bond distances (Å) and angles (°) for $[Zn_2(azil)_2(H_2O)_4]\cdot 2H_2O$. To be deposited.

D—H…A	d(D—H)	d(H…A)	d(D…A)	< (DHA)
O(1W)—H(1A)…O(3 W)	0.86(1)	2.1(1)	2.672(8)	126(11)
O(1W)—H(1B)…O(5)#1	0.86(1)	1.89(3)	2.714(7)	159(6)
O(2W)—H(2A)…N(1)#2	0.86(1)	1.87(3)	2.722(7)	169(15)
O(2W)—H(2B)…O(2)#3	0.86(1)	1.88(2)	2.726(8)	169(10)

Symmetry transformations to generate equivalent atoms: (#1) x + 1/2, −y + 1/2, z + 1/2; (#2) x, y + 1, z; (#3) −x + 1, −y + 1, −z + 1.

Table 4
Proposed assignments of the vibrational FTIR absorption spectra of azilsartan and the complex $[Zn_2(azil)_2(H_2O)_4]\cdot 2H_2O$ (ZnAzil). Wavenumber values in cm^{-1}.

Assignments	Azil	ZnAzil
νO−H	3425(s)	
νO−H water		3421 (m)
ν N−H	3226 (sh)	
ν C═O carboxylic acid	1773 (s)	
ν C═O oxadiazole	1692 (s)	1686 (s)
ν C═N+ ν_{as} **COO**$^-$	1613 (m)	1622 (s)
δip CCH arom + ν C═C (ring stretching)	1550 (s)	1550 (vs)
ν CN ip arom + ν CC	1519 (vw)	1522 (w)
ν CC + δ CCH ip + ν CN + δip (NH)	1490 (s) 1478 (s)	1491 (m) 1478 (m)
	1468 (s)	1461 (sh)
δ CCH ip + ν CN + δ COH	1438 (sh) 1432 (s)	1463 (vs), 1452 (sh)
	1413 (sh)	1435 (m) 1428 (sh)
		1409 (sh)
ν CC + δ CCH ip + ν_s **COO**$^-$	1389 (m) 1380 (sh)	1390 (vs)
CH_2 wag	1354 (s)	1355 (sh)
CH_2 wag + CH_2 rock + ν C−C bridge bond biphenyl + ν CO (COH)	1280 (s)1258 (s) 1242 (m)	1280 (m) 1243 (m)
ν CO	1160(m)	1152 (m)
δ CCHarom, CH_2 rock and wag	1146 (m)	1145 (sh)
ν ring, δ ip(C−H), δ ip(N−H)	1112 (m)1093 (m) @1082 (w)	1116 (w)1104 (w)
δ CCH ip arom + ring breath	1044 (s)	1040 (m)
δ CCH op arom + ν NO	878 (m) 818 (m)	872 (m) 819 (m)

vs, very strong; s, strong; m, medium; w, weak; sh, shoulder; vw, very weak; ip, in plane; op, out of plane; iph, in phase; op, out of phase; arom, aromatic ring.

complex are shown in Table 4 and Fig. 3.

Several main spectral features can be noted. The strong OH stretching of azilsartan at 3425 cm^{-1} due to the carboxylic group disappeared upon coordination because deprotonation of this group. A new band of medium intensity at 3421 cm^{-1} is assigned to the OH stretching of the crystallization and coordination water molecules of the metal complex. The absence of the strong C═O stretching band of the ligand at 1773 cm^{-1} in the zinc complex is also an indication of the deprotonation of the acid. The carboxylic acid group turns to a carboxylate moiety and the bands related to the antisymmetric and symmetric stretching modes are located at 1622 cm^{-1} and 1390 cm^{-1}, respectively. The difference $\Delta\nu = \nu_{as}(COO^-) - \nu_s(COO^-)$, is used as a criterion to establish the coordination of the COO^- group to the metal (Deacon and Phillips, 1980). The Δ value (ca. 232 cm^{-1}) is in concordance with a unidentate coordination mode of the carboxylate moiety. The C═O stretching bands of the oxadiazol group of the ligand remained in the same position and intensity on the complex, hence indicating that this group did not interact with the metal center. The NH stretching band of azilsartan at 3226 cm^{-1} is absent in the complex thus indicating the deprotonation and/or coordination of this group. These results are in agreement with the X-ray structural determinations and show that the ligand is negatively double-charged by the loss of two protons upon coordination. Besides, in the 3200 and 2600 cm^{-1} region, the ligand showed strong bands due to H-bonding.

3.3. Cell viability assay and stability measurements

The ZnAzil complex has been dissolved in DMSO (stock solutions, 2×10^{-5} M). These solutions were then diluted to the final concentrations indicated in the experimental part. To avoid cellular toxic effects of this solvent a 0.5% maximum DMSO concentration has been used (Maryam et al., 2017; Sharma et al., 2015).

The stability of the ZnAzil complex has been determined in DMSO, measuring the UV–vis spectra each 30 s. There was no observable variation in the electronic spectra of the DMSO solution of the complex at least during 90 min (ca. 3%, data not shown). These results demonstrated that during the manipulation time of the samples for the cellular determinations a significant amount of the complex remained without decomposition.

The cytotoxicity of $ZnSO_4$, azilsartan and ZnAzil on A549 cell line was determined by MTT assay. For comparison purposes cell viability has also been measured in the normal lung fibroblast cell line MRC5. As shown in Fig. 4, azilsartan induced no cytotoxicity to human lung cancer cells up to 250 μM concentration. The complex ZnAzil decrease cell viability in a dose-response manner. At 25 μM concentration, it can be observed a 65% of cell viability and this value is reduced to 21% at 500 μM. The calculated IC_{50} value after 24 h treatment was 155 ± 12 μM. In the MRC5 cell line, the compounds exerted weak cytotoxic effects up to 250 μM (Fig. 5). The measured effect of $ZnSO_4$ agrees with previous reports and has been added for comparative purposes (Zhao et al., 2015). The excess of Zn(II) ions (concentrations higher than 100 μM) is toxic in the A549 cancer cell line and one reason could be due to the production of oxidative stress (Zhao et al., 2015 and Fig. 6).

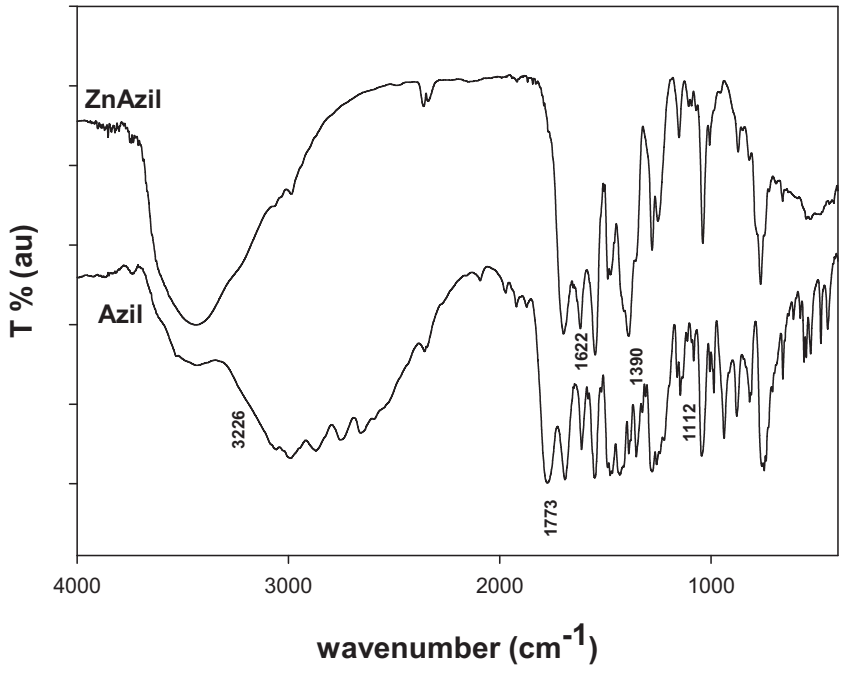

Fig. 3. FTIR spectra of azilsartan (Azil) and its Zn complex (ZnAzil); au: arbitrary units.

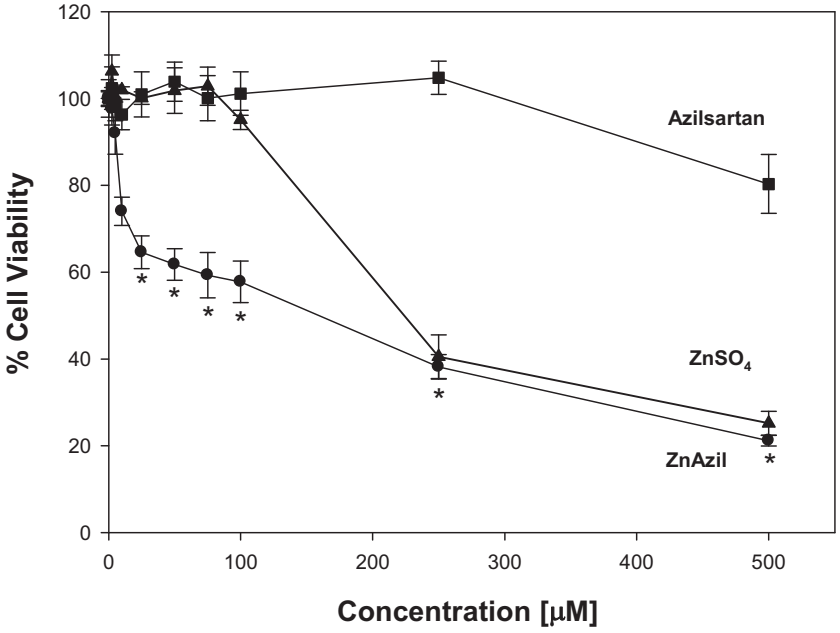

Fig. 4. Inhibitory effects of azilsartan (squares), $ZnSO_4$ (triangles) and ZnAzil (circles) on A549 cell viability. The cell line was treated with increasing concentrations of the compounds for 24 h. The results are expressed as the percentage of the basal level and represent the mean ± standard error of the mean (SEM) from three separate experiments. *Significant values in comparison with the control level ($P < 0.05$).

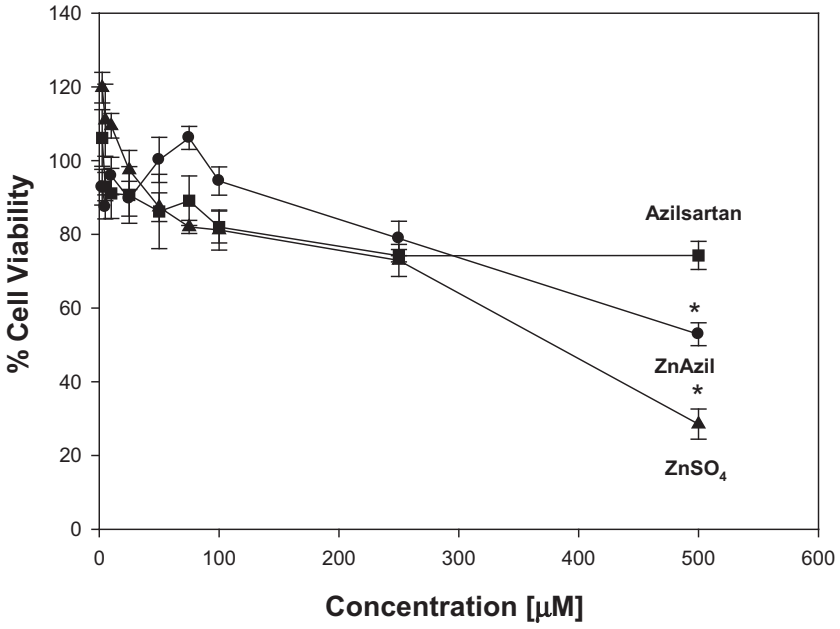

Fig. 5. Effects of azilsartan (squares), $ZnSO_4$ (triangles) and ZnAzil (circles) on MRC-5 cell viability. The cell line was treated with increasing concentrations of the compounds for 24 h. The results are expressed as the percentage of the basal level and represent the mean ± the standard error of the mean (SEM) from three separate experiments. *Significant values in comparison with the control level ($P < 0.05$).

3.4. Mechanism studies of cytotoxicity

3.4.1. ROS measurements

To examine whether the compounds may mediate their anticancer effects by oxidative stress, ROS levels were measured using H2DCFDA in a fluorometric analysis. ROS generation was measured following the treatment of malignant cells with $ZnSO_4$, Azilsartan and ZnAzil. The levels of DCFH-DA fluorescence in A549 cells treated with ZnAzil were markedly increased in a dose-dependent manner. The increment of ROS produced by $ZnSO_4$ was lower than that of the complex. Azilsartan produced low oxidative cellular stress at concentrations higher than 150 μM. It can be assumed that the free radicals decrease the concentration of important cellular compounds and cause weakness of the antioxidant system, making the cells more vulnerable to oxidative damage. Altogether, these results suggest that ZnAzil-induced generation of ROS play a significant role in ZnAzil-induced toxicity on A549 cancer cell line. Results of ROS assay are shown in Fig. 6.

On this basis, it is assumed that the oxidative stress may play a key role in the toxic effects. To confirm this hypothesis, the level of ROS generated by the compounds after a pre-incubation of the cells (30 min) with the antioxidant compound NAC (Fig. 7) was measured. It can be seen that when the cells were incubated in the presence of ROS suppressors the ROS levels were not altered. Besides, optical microscopy measurements showed that the compounds in the presence of NAC did not affect A549 cell viability (data not shown). Then, it can be demonstrated that oxidative stress is involved in the cell death mechanism.

3.4.2. Estimation of cell GSH and GSSG content

Glutathione (GSH) is the most abundant thiol-containing peptide antioxidant in mammals which neutralized free radicals and provides key source of reducing power in cells, being oxidized to glutathione

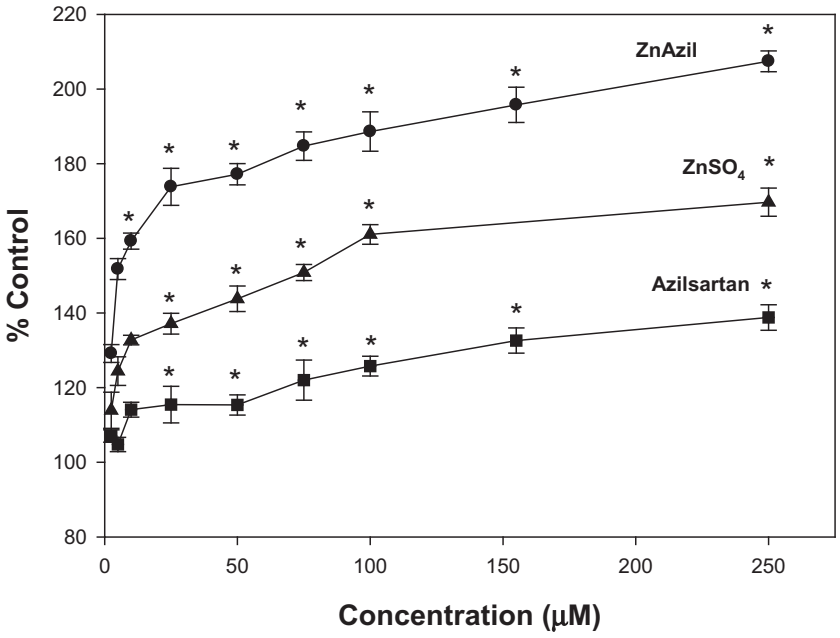

Fig. 6. Effect of azilsartan (squares), $ZnSO_4$ (triangles) and ZnAzil (circles) on ROS generation using the 2′,7′-dichlorodihydrofluorescein diacetate (H2DCFDA) probe. Negative control, DMSO. The values are expressed as a percentage of the control level and represent the mean ± SEM from three independent experiments. *Significant values in comparison with the control level ($P < 0.05$). #Significant values at the same concentration between azilsartan, $ZnSO_4$ and ZnAzil ($P < 0.05$).

disulfide (GSSG) (Biswas and Rahma, 2009). The ratio of GSH/GSSG is an essential marker to represent the redox state of cells. It is reasonable to suppose that the cellular GSH would decrease in oxidative stressed cells (Lu, 2013). To verify this hypothesis, we detected the levels of GSH and GSSG in the cancer cell line and the GSH/GSSG ratio was calculated. From Fig. 8 it can be seen that GSH levels and GSH/GSSG ratios were significantly decreased after ZnAzil treatment, suggesting that this compound induced depletion of GSH with the correspondent GSSG increment as ROS increases. Similarly, a small decrease in GSH levels and GSH/GSSG ratios was found for azilsartan. This finding suggests that the complex ZnAzil might make the cell more vulnerable to the oxidative stress producing an imbalance in the redox intracellular environment. Different mechanisms have been described to explain the induction of tumor cell death. Particularly, the generation of ROS may cause a series of cellular effects such as DNA cleavage and oxidative damage of different cellular components and finally triggers apoptosis.

3.4.3. Apoptosis and necrosis assay; cell morphology

Apoptosis or necrosis are the two major modes of cell death. Apoptosis is an active, programmed process and necrosis has been characterized as passive, accidental cell death resulting from acute cellular injury (Kryscko et al., 2008). The morphology associated with apoptosis was characterized by nuclear and cytoplasmic condensation, blebbing and cellular fragmentation into membrane-bound fragments. (Ziegler and Groscurth, 2004). Apoptotic cells undergo degradation of genetic and protein materials in the nucleus, and have their mitochondria break down, thus releasing cytochrome c. In contrast, necrotic cells swell or may form vacuoles on their surface, destroying the cell's processes and chemical structures. The unregulated release of cytochrome c and the cell membrane's phospholipid causes immediate reactions in surrounding tissues, leading to swelling and edema. To explore the underlying mechanisms on the mode of cell death, the effects of azilsartan, $ZnSO_4$ and ZnAzil were analyzed by AO/EtBr staining (Fig. 9). This technique revealed that ZnAzil treatment

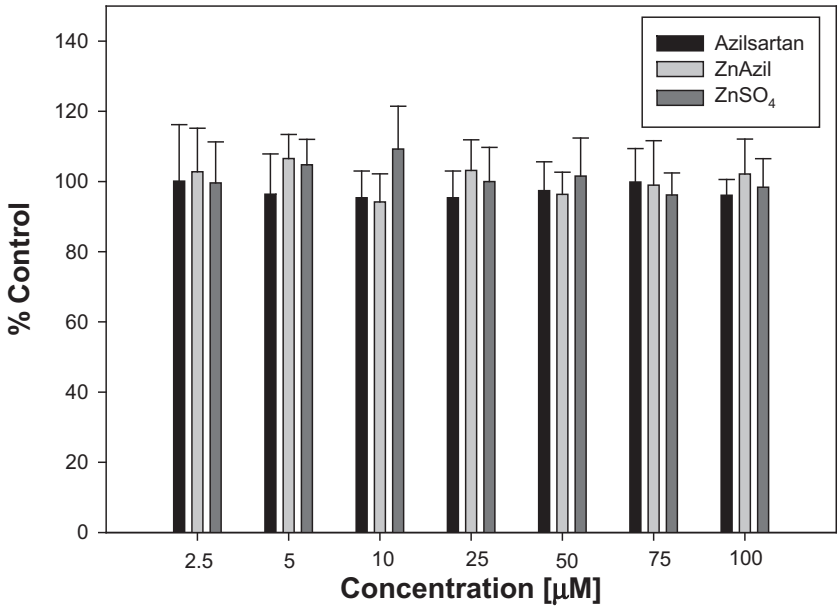

Fig. 7. Effect of N-acetylcysteine (NAC, 5 mM) on ROS production induced by azilsartan, ZnAzil and $ZnSO_4$. The values are expressed as a percentage of the control level and represent the mean ± SEM. All values are not different in comparison with the control level ($P < 0.05$).

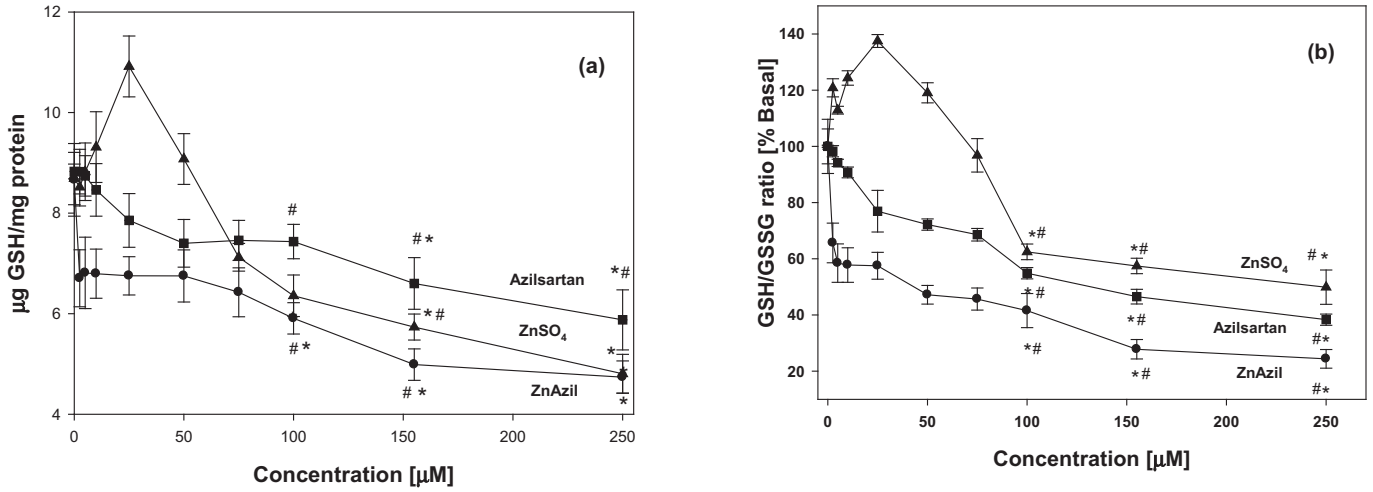

Fig. 8. µg of glutathione (GSH) per mg of protein (a) and GSH/GSSG ratio (b) as percentage of the basal level in A549 cells after treatment with azilsartan (squares), $ZnSO_4$ (triangles) and ZnAzil (circles) for 24 h. Each point represents mean ± S.D. of three independent experiments. *Significant differences versus basal $P < 0.05$. #significant differences at the same concentration between azilsartan, $ZnSO_4$ and ZnAzil, $P < 0.05$.

(155 µM) led to 50% of live cells, 49% of apoptotic cells and 1% of necrotic cells whereas the ligand induced only 3% of apoptotic cells and kept the remaining 97% alive. $ZnSO_4$ treatment at the same concentration generated 10% of apoptotic cells. Significant morphological changes upon ZnAzil treatment, compared to control and azilsartan treatment were observed. Chromatin condensation, cell shrinkage and apoptotic body formation could be seen and it was compatible with the apoptotic mechanism.

3.4.4. Western blot analysis

For the apoptotic pathways that cause cell suicide, the primary molecular signals are inactive proenzymes called caspases (cysteine-aspartic proteases) that proteolytically degrade a host of intracellular proteins to carry out the cell death program. The mitochondria are central regulators of apoptosis (Denning et al., 2002). Outer mitochondrial membrane proteins like Bax can from pores in the membrane to allow the release of cytochrome c (located in the intermembrane space). On the contrary other proteins like the Bcl-xL and Bcl-2 family act as anti-apoptotic members. They prevent the release of cytochrome c, thus inhibiting apoptosis (Goodsell, 2002).

The effects of 155 µM $ZnSO_4$, azilsartan and ZnAzil on the expression levels of Bax, Bcl-xL and caspase 9 signaling proteins were measured. As shown in Fig. 10, ZnAzil significantly elevated the expression of Bax and Caspase 9 in A549 cells compared to the control. The expression level of Bax and Caspase 9 in the $ZnSO_4$ treatment was slightly higher than the control. However, no significant changes in Bax and caspase 9 expressions were observed in cells treated with azilsartan in comparison with the control.

The level of Bcl-xL expression was decreased in cells treated by ZnAzil and was found slightly increased after azilsartan treatment. Bax/Bcl-xL ratios were calculated and show that it was significantly increased in A549 cells treated by ZnAzil.

Then, it can be concluded that high expression of Bax and Caspase 9 in the cells incubated with ZnAzil demonstrated that it has proapoptotic enhancer effects inducing an intrinsic apoptotic pathway on the A549 cancer cell line. Likewise, our data showed that ZnAzil treatment reduced the expression of Bcl-xL protein. The increase of Bax/Bcl-xL ratio causes caspase-9 activation, the loss of cell viability and enhanced apoptosis.

3.5. Bovine serum albumin (BSA) interactions

Drug-plasma protein binding may greatly influence the bioavailability and metabolism of a plasma-transported drug and the complex between albumin and a compound could be partially protected from the metabolism of the unbound drug. Then, it is important to determine the value of the binding constant and the nature of the interaction mode between albumin and different drugs. Albumin is the major transport protein in blood for Zn^{2+}. It modulates zinc uptake by endothelial cells and facilitates uptake of Zn^{2+} by erythrocytes. Results of binding experiments done at several pH values suggested that histidyl residues appear to be involved in zinc binding. The concentration of Zn^{2+} in blood plasma is near 19 µM, most of which is bound to albumin. The log K for the bovine serum albumin-Zn^{2+} interaction was calculated to be 7.28 (Masuoka et al., 1993) and the value of the Stern-Volmer constant of quenching of intrinsic fluorescence of BSA and Zn^{2+} has been measured (K_{sv} $ZnSO_4$ = 529 ± 15 L mol^{-1}) (Plotnikova et al., 2016). In addition, azilsartan medoxomil and its metabolites are highly bound to plasma proteins and the major binding protein of azilsartan was albumin in human plasma. The distribution of azilsartan into blood cells of animals and in humans is very limited (< 5%). After oral administration of azilsartan the bioavailability was 75% in humans. No quantitative data on the interaction of azilsartan with albumin have been reported (Angeli et al., 2013). Therefore, we have measured the interaction of azilsartan and its ZnAzil complex with BSA.

The fluorescence spectra of BSA show a broad band with maximum at 336 nm and the compounds displayed a fluorescence peak at 368 nm. It is observed that the fluorescence intensity of BSA decreases with increasing concentration of azilsartan and its Zn complex. Both fluorescence spectra showed a broad band with maximum at 368 nm, its intensity increased with increasing concentration of the compounds and therefore, we have assigned the observed shoulder to their fluorescence (Fig. 11).

When the fluorescence emission spectra of BSA with the addition of the compounds have been corrected by spectral deconvolution into two Gaussian components, the bands originating from the emission of the compounds were not visible (Fig. 12).

The corrected spectra are shown in Fig. 13 and a decrease of fluorescence intensities of BSA with the increase of the concentration of the compounds can be observed.

To confirm the quenching mechanism the fluorescence data at different temperatures have been analyzed with the Stern-Volmer equation (Lakowicz, 2013):

$$F_0/F = 1 + K_q\tau_0[Q] = 1 + K_{SV}[Q] \quad (1)$$

where F_0 and F are the fluorescence intensities in the absence and

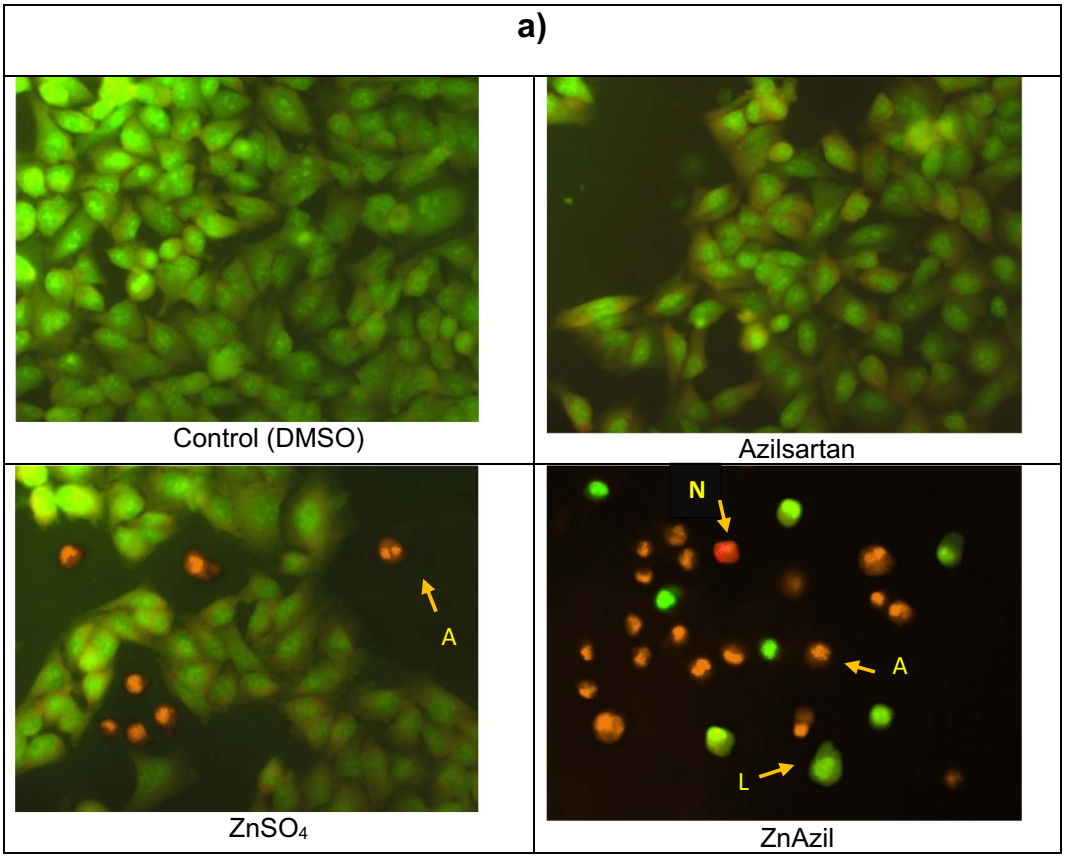

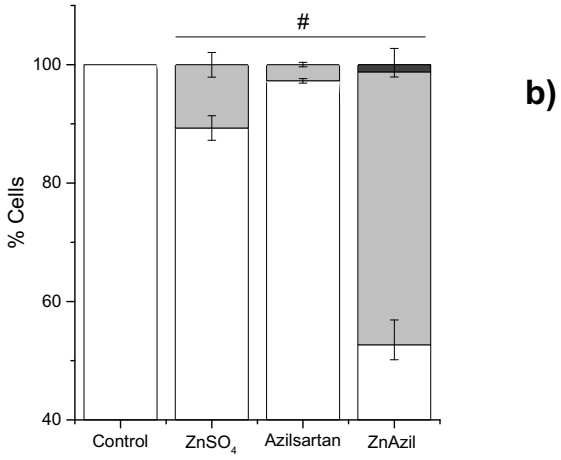

b)

Fig. 9. (a) Representative photomicrographs of the morphological changes in A549 cells treated with 155 μM (IC_{50}) of azilsartan, $ZnSO_4$ and ZnAzil followed by Acridine Orange/Ethidium Bromide staining. A total of 200 cells were analyzed and counted in three independent experiments. Images are magnified at 400×. L: live A: apoptotic, N: necrotic (b) Bars represent percentages of cells that were viable (white), apoptotic (gray), and necrotic (black) cells. Values are mean ± SEM. #significant differences at the same concentration between azilsartan, $ZnSO_4$ and ZnAzil $P < 0.05$.

presence of quencher, respectively; K_q is the bimolecular quenching constant; τ_0 is the lifetime of the fluorophore in the absence of quencher; [Q] is the concentration of quencher and K_{sv} is the Stern-Volmer quenching constant which can be obtained from the slope of Eq. (1). The Stern-Volmer plots are shown in Fig. 14.

At concentrations between 0 and 20 μM, the average values of Ksv are obtained from the slopes of a linear regression (see Table 5). The fluorescence lifetime τ_0 of the biopolymer is taken as 1.0×10^{-8} s. The quenching rate constant K_q was calculated and listed in Table 5. All K_q values resulted higher than those obtained for maximum scattering collision (dynamic) quenching of various quenchers with biopolymers (2.0×10^{10} L mol^{-1} s^{-1}), indicating a static quenching initiated by formation of a complex in the studied concentration range (Lakowicz, 2013).

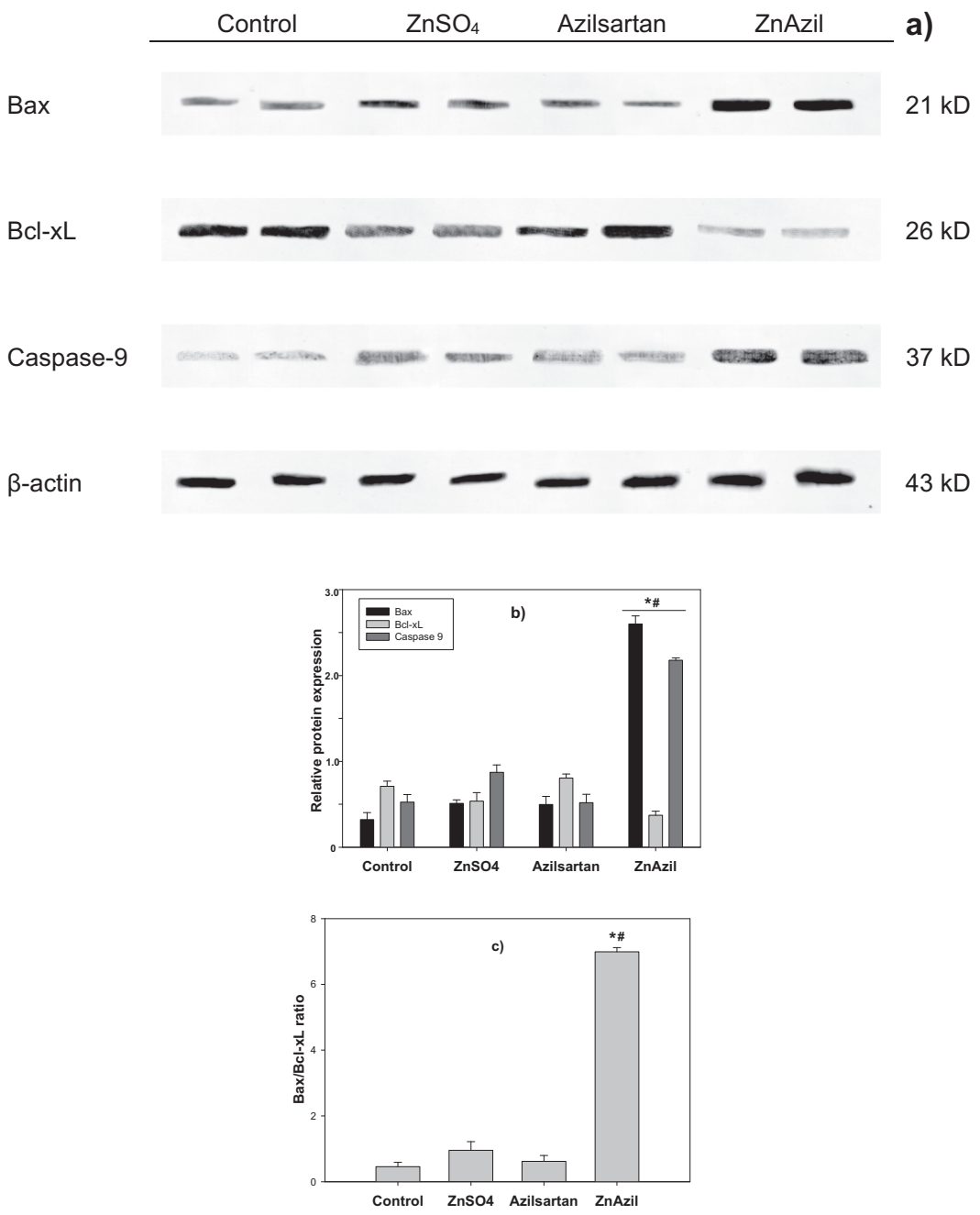

Fig. 10. (a) Immunoblotting analysis on the expression of Bax, Bcl-xL and Caspase 9 in A549 cells treated by 155 μM of $ZnSO_4$, azilsartan, ZnAzil. β-Actin was used as internal control. Three independent experiments were carried out. Two representative bands of each sample are shown. (b) Densitometry analysis of the correspondent protein bands. (c) BAX/BCL-xL ratio. *Significant values in comparison with the control level ($P < 0.05$). #Significant values at the same concentration between azilsartan, $ZnSO_4$ and ZnAzil ($P < 0.05$).

3.5.1. Binding constants and the number of binding sites

The value of the binding constant, K_a, is essential to correlate with the transport, disposition and in vivo efficacy of the compound and to understand the distribution of compounds in plasma. A weak binding can result in comparatively high concentrations of the drug in the plasma, resulting in a shorter life time while a strong binding can decrease the concentrations of compound in plasma, improving the pharmacological effect. For static quenching (complex formation between protein and quencher), the following equation was used to calculate the binding constant and binding sites (Lakowicz, 2013).

$$\log[(F_0 - F)/F] = \log K_a + n \log[Q] \quad (2)$$

where K_a and n are the binding constant and binding site number, respectively. The plots of log $[(F_0 - F) / F]$ vs log [Q] presented in Fig. 15 are linear. Binding constants (K_a) and the binding site number (n) could be calculated from the intercept and slope (Table 5). It can be seen that the binding constants decreased with an increase in temperature, resulting in a reduction of the stability of the binding between BSA and the compound. The results obtained from the graph of the inverse correlation between K_a and temperature indicated, again, that the mechanisms of the fluorescence quenching of BSA induced by azilsartan and ZnAzil are static and not a dynamic process. Furthermore, the constants are in the intermediate range suggesting that azilsartan and ZnAzil could be bonded and transported by BSA.

3.5.2. Nature of the interaction mode

The interaction of BSA with the compounds may involve hydrophobic forces, electrostatic forces, Van der Waals, Hydrogen bonds and

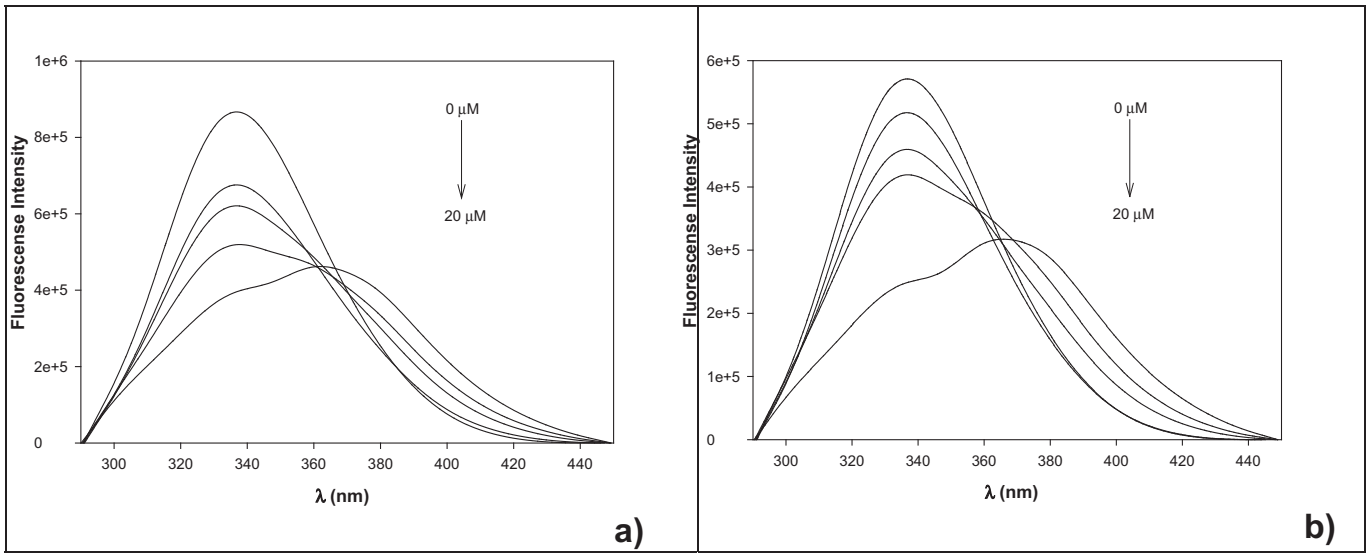

Fig. 11. BSA fluorescence spectra at different concentrations of azilsartan (a) and ZnAzil (b). λ_{ex} = 280 nm, T = 298 K. Each experiment was performed in triplicate and at least three independent experiments were carried out.

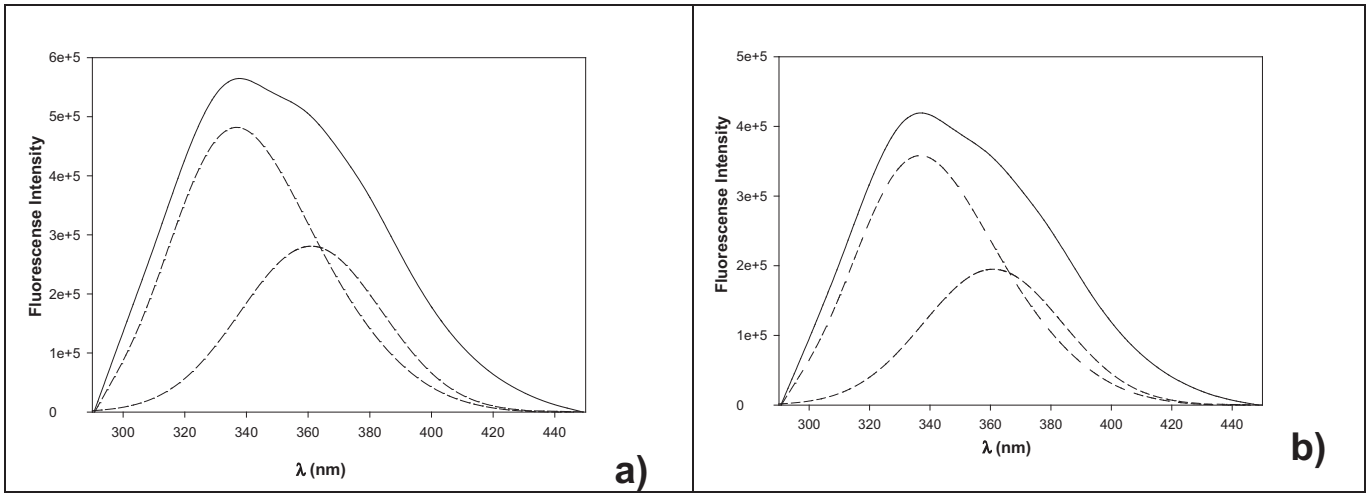

Fig. 12. Examples of BSA-Azilsartan (a) and BSA-ZnAzil (b) emission spectra deconvoluted into two Gaussian components by the curve-fitting method. Excitation wavelength was 280 nm. Solid lines, measured spectra; dashed, separate components. The peaks corresponding to BSA (λ_{max}: 336 nm) azilsartan, ZnAzil (λ_{max}: 368 nm) were adjusted using OriginPro 9.1.0 software.

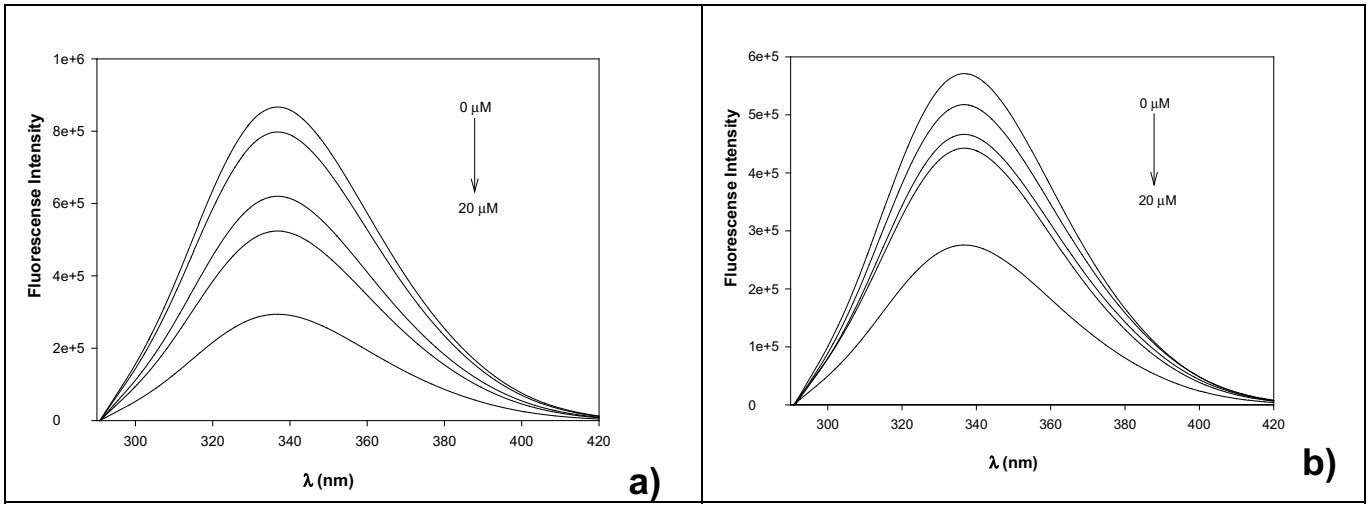

Fig. 13. BSA fluorescence after the fitting and deconvolution processes of the spectra at different concentrations of azilsartan (a) and ZnAzil (b). λ_{ex} = 280 nm, T = 298 K.

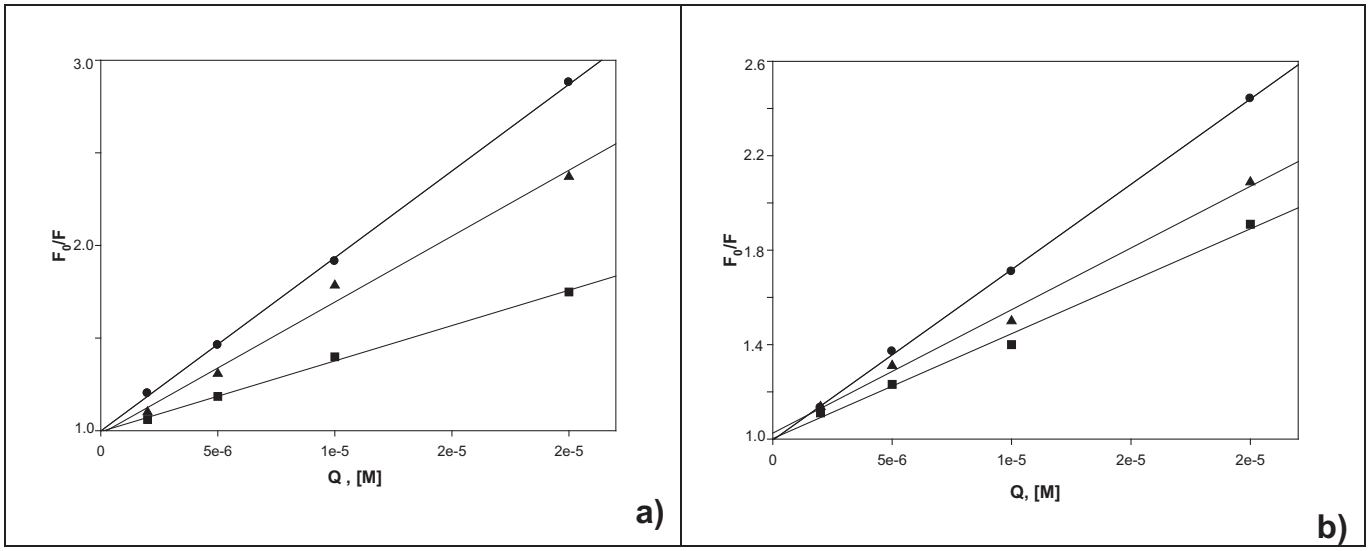

Fig. 14. Plots of F_0/F vs [Q] for BSA with azilsartan (a) and ZnAzil (b) at different temperatures ((●), 298 K; (▲), 303 K; (■), 310 K), λ_{ex} = 280 nm. Each experiment was performed in triplicate and at least three independent experiments were carried out.

Table 5
Stern-Volmer constant (K_{sv}), quenching rate constant (K_q), binding constant (K_a) and n binding sites for the interaction of azilsartan and ZnAzil with BSA (6 μM) in Tris–HCl buffer (0.1 M, pH 7.4).

Compounds	T (K)	$K_{sv}(\times 10^4)$ (L mol^{-1})	r^2	K_q ($\times 10^{12}$) (L mol^{-1} s^{-1})	K_a ($\times 10^5$) (L mol^{-1})	n
Azilsartan	298	9.35 ± 0.13	0.9995	9.35 ± 0.13	3.29 ± 0.21	1.13 ± 0.02
	303	7.11 ± 0.04	0.9886	7.11 ± 0.04	1.40 ± 0.24	1.03 ± 0.03
	310	3.81 ± 0.9	0.9956	3.81 ± 0.90	0.59 ± 0.14	0.95 ± 0.05
ZnAzil	298	7.22 ± 0.03	0.9965	7.22 ± 0.03	0.99 ± 0.07	1.01 ± 0.03
	303	5.22 ± 0.05	0.9937	5.22 ± 0.05	0.63 ± 0.15	0.96 ± 0.02
	310	4.44 ± 0.01	0.9919	4.44 ± 0.01	0.38 ± 0.2	0.95 ± 0.07

r^2 is the correlation coefficient for the K_{SV} values.

other interactions. It is suggested that from the changes in the thermodynamic parameters (ΔH and ΔS) the mode of interaction can be assessed. If ΔH > 0 and ΔS > 0, hydrophobic interaction occurs, and if ΔH < 0 and ΔS < 0, Van der Waals and Hydrogen bonds dominated, and if ΔH < 0 and ΔS > 0, electrostatic forces dominated (Ross and Subramunian, 1981). If ΔH does not vary significantly over the temperature range studied, then its value and that of ΔS can be evaluated from the van't Hoff equation (Eq. (3)):

$$\ln K_a = -\Delta H/RT + \Delta S/R \quad (3)$$

where K_a is analogous to the associative binding constants at the corresponding temperature and R is the gas constant. The free energy change (ΔG) is then estimated from the following relationship (Eq. (4)):

$$\Delta G = \Delta H - T\Delta S \quad (4)$$

The calculated thermodynamic values are listed in Table 6. The negative ΔG value clearly defines a spontaneous reaction. The negative

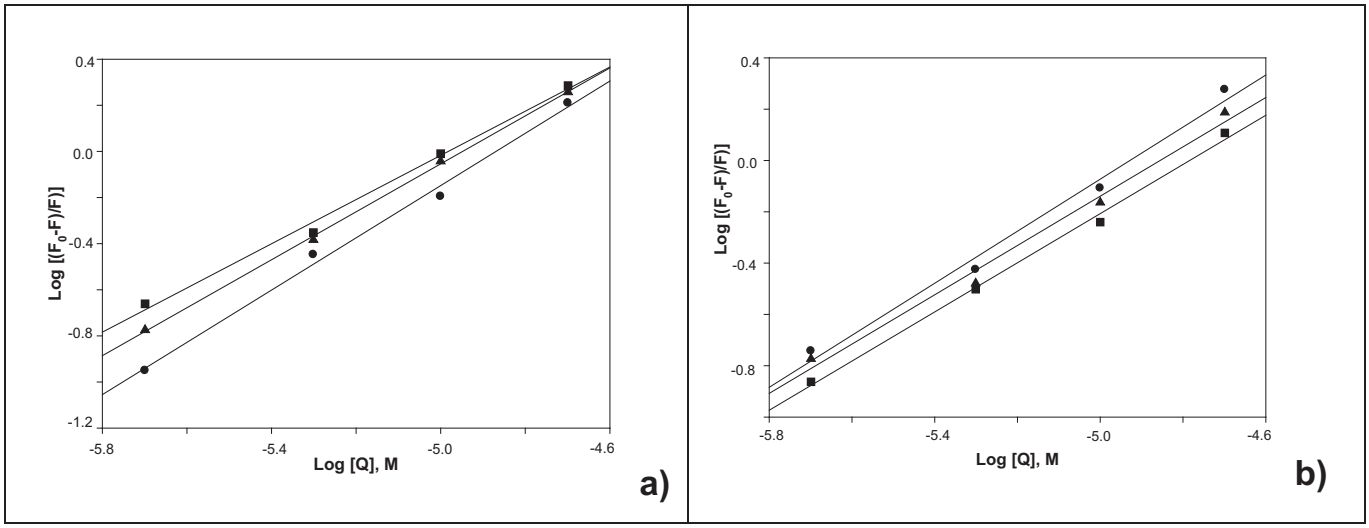

Fig. 15. Plots of log(F_0 − F) / F vs. log [Q] for BSA with azilsartan (a) and ZnAzil (b) at different temperatures: (●) 298 K; (▲) 303 K; (■) 310 K, λ_{ex} = 280 nm.

Table 6
Thermodynamic parameters for the interactions between azilsartan and ZnAzil with BSA.

Compounds	ΔH (KJ/mol)	ΔS (J/mol)	ΔG (KJ/mol)
Azilsartan	−108.53	−258.93	−31.36(298 K) −30.07(303 K) −28.26 (310 K)
ZnAzil	−61.14	−109.71	−28.44 (298 K) −27.89 (303 K) −27.12 (310 K)

values of ΔH and ΔS suggest Van der Waals and Hydrogen bonding drives mainly the interaction between BSA and the compounds. Giving the structure of azilsartan and ZnAzil and tryptophan and tyrosine, it is reasonable to expect π-π interactions between the aromatic rings on BSA and the compounds.

4. Discussion

Cancer cells exhibit a higher and more persistent oxidative stress level compared to normal cells, rendering malignant cells more vulnerable to being killed by drugs that increase ROS levels. Normal cells have lower basal intracellular ROS levels and a full antioxidant capacity, being less vulnerable to the induction of oxidative stress by the compounds (Gibellini et al., 2012; Szatrowski and Nathan, 1991; Toyokuni et al., 1995). Accordingly, weak cytotoxic effects of the compounds up to 250 μM were displayed in the MRC5 cell line (Fig. 5).

The effects for the Zn(II) ions have been described in murine fibroblasts and human lung epithelial cells and could be explained by the activation of MAP kinase in the presence of concentrations of extracellular zinc which exceed the capacity of homeostatic control and may be at least partially caused by the inhibition of protein tyrosine phosphatase (IC_{50} value, 200 μM) (Beyersmann and Haase, 2001). On the other hand, zinc (II) cation has beneficial roles in the respiratory epithelium, acting as an anti-oxidant, microtubule stabilizer, anti-apoptotic, growth cofactor and anti-inflammatory agent (Truong-Tran et al., 2000). Regarding Zn(II) complexes, recent studies have shown that they have not exerted significant cytotoxic effects on the MRC-5 cells (Anđelković et al., 2017; Konidaris et al., 2013). Moreover, and concerning the AT1 antagonists, it has been reported that did not affect the viability of lung fibroblasts (Okada et al., 2009) and that the AT1 antagonist losartan abolished the increase in ROS in renal and endothelial cells produced by Ang II. (Pendergrassa et al., 2009; Bian et al., 2017). Furthermore, studies in patients with hypertension showed that losartan decreased oxidative stress in serum after exposure to hypoxia (Pialoux et al., 2011), improving the endothelial function (Flammer et al., 2007). Moreover, a combination of an AT1 antagonist and a lipid-lowering medication (statin), generated a decrease of Ang II-induced ROS and inflammation (Akershoek et al., 2017). Even in smoker patients, the use of losartan reduced oxidative stress and ameliorates the lung injury (Podowski et al., 2012). The antioxidant protection of cardiac, lung and liver function due to AT1 blockade has also been demonstrated by the increase of GSH level and the ratio GSH/GSSG (Khaper and Singal, 2001). In addition, a variety of recent studies described the role of AT1 receptors in apoptosis. Ang II induced apoptosis in human and rat alveolar epithelial cells (Wang et al., 1999) and this event could be reversed by the administration of angiotensin antagonists (Uhal et al., 2003). Likewise, losartan could prevent caspase 3 activation and produced inhibition of apoptosis in lung cells (Li et al., 2003). Hence, the mechanism of action of the compounds was not studied in the normal lung fibroblast cells, because the viability of this cell line was practically not affected by 250 μM concentration of the compounds, in agreement with the evidence in literature.

The angiotensin II receptor blockers showed low cytotoxic effects in cancer cell lines (except telmisartan) and no cytotoxic effects in human fibroblasts (see Table 7).

There are few examples in the literature of the cytotoxic effects of metal-sartan complexes. An improvement of the cytotoxic effects has been found when the structure of the antihypertensive agents was modified by metal complexation. (Williams, 2013). We have previously studied the anticancer effects of other sartans bounded to copper(II). Higher cytotoxic effects of these coordination complexes (with losartan, candesartan, valsartan, telmisartan and irbesartan) with respect to their parent antihypertensive drugs have been found. At the tested concentrations valsartan did not show cytotoxic effects on two osteoblastic cell lines in culture (one normal MC3T3E1 and one tumoral UMR106) and the copper complex behaved as a cytotoxic compound in the cancer cell line. In the same cell lines, the Losartan-copper complex exerted more cytotoxic effects in the UMR106 line than the copper(II) ion and Losartan. (Etcheverry et al., 2007, 2012). Besides, in the LNCaP, DU145 and PC3 human prostate cancer cell lines the copper complex with telmisartan resulted more cytotoxic than that of irbesartan. The effect was more pronounced for the LNCaP cell line. Both candesartan and its copper(II) complex displayed low cytotoxic effects in the three tested cell lines. (Islas et al., 2013, 2014, 2016).

On the other hand, some chemoterapy medications used to treat a number of types of cancer showed IC_{50} values for the A549 tumor cell line (72 h drug exposure) in the range of 10^{-7}–10^{-10} M: Gemcitabine (2.8×10^{-10} M), Vincristine (2.5×10^{-7} M), Paclitaxel (4.0×10^{-8} M), Bortezomib (3.1×10^{-9} M), Topotecan (8.0×10^{-7} M), Docetaxel (3.0×10^{-9} M), Etoposide (7.8×10^{-7} M), while for others the IC_{50} values ranged between 10^{-3} to 10^{-6} M: Carmustine (1.0×10^{-3} M), Oxaliplatin (9.0×10^{-4} M), Dacarbazine (6.0×10^{-4} M), Fluorouracil (9.2×10^{-5} M), and Cyclophosphamide (1.0×10^{-3} M) (Moneo Ocaña et al., 2012). The IC_{50} value of 1.55×10^{-4} M obtained for the ZnAzil complex at 24 h incubation showed that the complex exerted anticancer effects like the second group of the selected drugs.

Concerning the mechanism of action, it is known that cellular redox status is a consequence of the balance between the ROS levels and endogenous thiol buffers, such as glutathione, which protect cells from oxidative stress. Higher ROS contents exceeding compensatory changes lead to the activation of apoptotic effector mechanisms. ROS are generated by the treatment with cytotoxic drugs and selectively kill cancer cells by the abrogation of proliferative signals (Davis et al., 2000), producing changes in the inner mitochondrial membrane permeability. This change of permeability causes the loss of the mitochondrial transmembrane potential (ΔΨm) and the release of pro-apoptotic proteins (Indran et al., 2011). Apoptotic events are highly regulated by the Bcl-2 family. One of the members of this family is Bcl-xL which protects the cells by interacting with mitochondrial proteins thus preventing the formation of mitochondrial pores, protecting membrane integrity and inhibiting the release of apoptogenic factors such as cytochrome c (Brenner et al., 2000). Bax is a pro-apoptotic protein that resides in the cytosol under physiological conditions. An apoptotic trigger can lead to its translocation to the mitochondria. Bax can homodimerize or heterodimerize with other pro-apoptotic members thus disrupting the integrity of the outer mitochondrial membrane, generating pores and increasing its permeability. These pores can then lead to the release of apoptogenic factors such as cytochrome c (Vyssokikh et al., 2002). Bax and Bcl-xL antagonize the apoptotic cascade.

This intrinsic pathway of cell death is especially susceptible to ROS. Intracellular ROS production causes intracellular acidification. The change in cytosolic pH influences the conformational status of Bax, resulting in its activation and oligomerization at the mitochondria, thereby facilitating the release of apoptotic factors (Lagadic-Gossmann et al., 2004). Following the release of cytochrome c, a complex known as apoptosome is formed which recruit and activate caspase-9 (Boatright and Salvesen, 2003). Activated caspase-9 will then cleave and activate downstream the executioner caspases such as caspase-3, and -7. Hence, the biochemical activation of the components of the cell death program is responsible for the morphological changes observed in apoptosis, including mitochondrial damage, nuclear

Table 7
Cytotoxic effects of azilsartan, Zn-azil, Zn(II), losartan, telmisartan, olmesartan and candesartan. Comparative IC_{50} values of various ARBs in different Human carcinoma and fibroblast cell lines. Cell lines, HFF: Human foreskin fibroblasts; HeLa: Human cervical cancer cells; PC3: Human Prostatic Small Cell Carcinoma; HMEC's: 184A1 human mammary epithelial cells; PRTECs: proximal tubular endothelial cells

	Azilsartan	Znazil	Zn	Losartan	Telmisartan	Olmesartan	Candesartan
Human carcinoma	No cytotoxic effects (A549)	155 ± 12 μM (A549)	221 ± 25 μM (A549)	210.46 ± 15.67 μM[a] (A549)	80.37 ± 10.64 μM[a] (A549)	486 μM[b] (HeLa)	No cytotoxic effects[c] (PC3)
Human Fibroblasts	No cytotoxic effects (MRC-5)	No cytotoxic effects (MRC-5)	378 ± 17 μM (MRC-5)	No cytotoxic effects[d] (HMEC's)	No cytotoxic effects[e] (PRTECs)	No cytotoxic effects[b] (HFF)	No cytotoxic effects[d] (HMEC's)

[a] Godugu et al., 2013.
[b] Bakhtiar et al., 2015.
[c] Alhusban et al., 2014.
[d] Piastowska-Ciesielska et al., 2014.
[e] Funao et al., 2009.

membrane breakdown, DNA fragmentation, chromatin condensation, and the formation of apoptotic bodies (Budihardjo et al., 1999). We found that ROS levels were significantly enhanced in A549 cells after 24 h treatment with ZnAzil, which could have led to change the mitochondrial membrane permeability. Our observations also suggested that ROS production blocked cell growth and induced apoptosis through the ROS-mediated intrinsic pathway. Bcl-2 family proteins also play an important role and represent essential targets in cancer therapy (Lessene et al., 2008). An up regulation of pro-apoptotic protein Bax with concomitant decrease of antiapoptotic Bcl-xL in ZnAzil treated cells has been observed. Besides, a significant higher Bax/Bcl-xL ratio in groups treated with ZnAzil compared to azilsartan, Zn(II) and untreated controls has been determined by densitometric analysis. Our data demonstrates that ZnAzil induces activation of caspase-9. These results, supported with acridine orange and ethidium bromide double-staining and the study of the apoptotic morphology, suggest that ZnAzil induces formation of apoptosome and activates caspase cascade in the mitochondrial apoptotic pathway.

In summary, the inhibitory effect of the new coordination compound ZnAzil on the viability on lung cancer through induction of apoptosis has been determined. The molecule triggers intrinsic apoptotic pathway by generating ROS and modulating expression of Bcl-2 family proteins, leading to apoptosome mediated activation of caspase cascades. However, further studies are needed to elucidate the mechanism in a comprehensive manner.

In addition, it is well known that drugs used in pharmaceutics require stabilization against oxidation or degradation process. For that reason, binding them to carriers with high affinity and selectivity for targeting to the right environment and subsequent controlled release is highly beneficial. In this regard, proteins often possess one or more of these properties. In particular, albumin, the most abundant protein in the circulatory system with ability in reversibly binding to a wide range of ligands has been used for this objective (De Wolfi and Brett, 2000). Indeed, albumin is actually used as a carrier protein for the treatment of various diseases, rheumatoid arthritis, diabetes, hepatitis, among others. In cancer, for instance, serum albumin have been used for the delivery of cisplatin, doxorubicin and 5-fluorouracil to tumors in the liver, breast, and lungs, being the albumin-bound drugs more effective than free drug (De Wolfi and Brett, 2000, Kratz and Elsadek, 2012). Bearing in mind that the binding to the albumin can modify pharmacokinetic and pharmacodynamic properties of drugs, the determination of the binding sites and their relative affinities for different compounds is an important aspect in drug development.

Bovine serum albumin (BSA) has high homology and similarity to the human serum albumin in sequence and conformation (He and Carter, 1992), it is cheap and readily available, and thus it is widely used as a model protein to study the ligand-protein interactions. The fluorescence of this protein is caused by tryptophan, tyrosine and phenylalanine residues, and is highly susceptible to its local chemical environment and temperature. When the protein is excited at 280 nm, most of the fluorescence emissions are due to excitation of tryptophan residues with little emission from tyrosine and none from phenylalanine. Fluorescence quenching refers to any process that decreases the fluorescence intensity of a fluorophore due to a variety of molecular interactions including excited state reactions, molecular rearrangements, energy transfer, ground state complex formations and collision quenching. Then, fluorescence quenching measurements have been widely used to study the interactions of compounds with this protein (Lakowicz, 2013).

The usual typical association constants for the binding of drugs to one or very few high-affinity sites of BSA are in the range of 10^4–$10^6\ M^{-1}$ (Kragh-Hansen et al., 2002; Carter and Ho, 1994; Kragh-Hansen, 1981). But additionally to the primary site(s), several sites of lower affinity are available. For this reason the range 10^3–$10^6\ M^{-1}$ is commonly accepted and there are examples in the literature with binding constant values $\sim 10^3\ M^{-1}$ (Zhang et al., 2011). For instance, considering the chemotherapy medication cisplatin that is used to treat many different types of cancer, different data appeared in literature according to several factors like cisplatin/albumin ratio, incubation time, etc. Nevertheless, an association constant calculated for the cisplatin-HSA complexes showed a weak *cis*-Pt–protein interaction ($K = 8.52 \times 10^2\ M^{-1}$, by spectrophotometric determination). For other anticancer drugs the K values appeared at ca. $10^3\ M^{-1}$ (equilibrium dialysis or ultrafiltration techniques) (Finlay and Baguley, 2000). Hence, the binding constants of azilsartan and its Zn complex with BSA were determined to be in the usual range of pharmacological drugs.

The measurement of the binding constants at different temperatures is a usual procedure in fluorescence experiments to analyze if the quenching processes are statics or dynamics (Lakowicz, 2013). It has been assumed that higher temperatures produced faster diffusion and hence larger amounts of collisional quenching. Higher temperatures will result in the dissociation of weakly bound complexes. Therefore, it could be established, that the binding constants calculated at 310 K (ca. $10^4\ M^{-1}$), is a typical association constant for drug binding.

5. Conclusions

A new metal complex between the antihypertensive drug azilsartan and the biometal Zn(II) has been synthesized and characterized with the aim to study the structural modifications in the drug produced by its binding to the metal. While the administration of azilsartan did not produce anticancer effects up to 250 μM concentrations, the new complex produced an increase in cancer cell ROS levels and a decrease of GSH and the GSH/GSSG ratio that have been associated with cell death or membrane injury. High levels of ROS can induce apoptosis by

activating the mitochondrial-mediated apoptotic pathway. The elevation of oxidative stress may trigger mitochondrial permeability transition pore opening, cytochrome c release, caspase cascade activation, and apoptosis. Herein we have determined a pro-apoptotic activity of ZnAzil. The study of the protein expression levels induced by ZnAzil showed that the compound up-regulated caspase 9 and Bax and produced down-regulation of Bcl-xL suggesting a mitochondrial dependent intrinsic pathway of action. It has then been demonstrated that the complexation of the antihypertensive drug azilsartan with Zn(II) improved the anticancer activity of the ligand on the human lung cells. Owing to the biological and biochemical differences between cancerous and normal cells, these substances can achieve selectivity of treatment, while maintaining a weak or null impact on normal cells. Therefore, ZnAzil could be a potential candidate for further evaluation of other cancer cell lines since it is deleterious for the human lung cancer cells but is less toxic to the normal lung related cells (MRC5). Fluorescence spectroscopy was used to investigate the binding mechanism, number of binding sites, binding constants and thermodynamic parameters in the presence azilsartan and ZnAzil. The results indicated that the compounds bind to BSA with moderate affinity, the intrinsic fluorescence of BSA was quenched through static quenching mechanism and Van der Waals and hydrogen bonds interactions played the main role in the binding of the antihypertensive drug and its Zn complex to BSA.

Transparency document

The Transparency document associated with this article can be found, in online version.

Acknowledgments

This work was supported by CICPBA, UNLP (Project 11/X709, 11/X736), CONICET (PIP 0611, 0651) and ANPCyT (PICT-13-0569, PME-06-2804 and PICT-06-2315) of Argentina. VRM is fellowship holder from ANPCyT. EGF, GAE and OEP are research fellows of CONICET. PAMW is a research fellow of CICPBA, Argentina.

Appendix A. Supplementary data

Supplementary Information Available. Tables of fractional coordinates and equivalent isotropic displacement parameters of the non-H atoms (Table S1), full bond distances and angles (Table S2), atomic anisotropic displacement parameters (Table S3) and hydrogen atoms positions (Table S4). Crystallographic structural data have been deposited at the Cambridge Crystallographic Data Centre (CCDC). Any request to the Cambridge Crystallographic Data Centre for this material should quote the full literature citation and the reference number CCDC 1533017. Supplementary data associated with this article can be found in the online version, at https://doi.org/10.1016/j.tiv.2018.01.009.

References

Aguirre, M.V., Juaristi, J.A., Alvarez, M.A., Brandan, N.C., 2005. Characteristics of *in vivo* murine erythropoietic response to sodium orthovanadate. Chem. Biol. Interact. 156, 55–68.

Akershoek, J., Brouwer, K., Vlig, M., Boekema, B., Beelen, R., Middelkoop, E., Ulrich, M., 2017. Differential effects of losartan and atorvastatin in partial and full thickness burn wounds. PLoS One 12 (6), e0179350. http://dx.doi.org/10.1371/journal.pone.0179350.

Alhusban, A., Al-Azayzih, A., Goc, A., Gao, F., Fagan, S.C., Somanath, P.R., 2014. Clinically relevant doses of candesartan inhibit growth of prostate tumor xenografts in vivo through modulation of tumor angiogenesis. J. Pharmacol. Exp. Ther. 350, 635–645. http://dx.doi.org/10.1124/jpet.114.216382.

Anđelković, K., Milenković, M., Pevec, A., Turel, I., Matić, I., Vujčić, M., Sladić, D., Radanović, D., Brađan, G., Belošević, S., Čobeljić, B., 2017. Synthesis, characterization and crystal structures of two pentagonal-bipyramidal Fe(III) complexes with dihydrazone of 2,6-diacetylpyridine and Girard's T reagent. Anticancer properties of various metal complexes of the same ligand. J. Inorg. Biochem. 174, 137–149. http://dx.doi.org/10.1016/j.jinorgbio.2017.06.011.

Angeli, F., Verdecchia, P., Pascucci, C., Poltronieri, C., Reboldi, G., 2013. Pharmacokinetic evaluation and clinical utility of azilsartan medoxomil for the treatment of hypertension. Expert Opin. Drug Metab. Toxicol. 9, 379–385.

Bakhtiar, E., Hosseini, A., Boroushak, T., Mousavi, S., 2015. Synergistic, cytotoxic and apoptotic activities of olmesartan with NF-κB inhibitor against HeLa human cell line. Toxicol. Mech. Methods 25, 8. http://dx.doi.org/10.3109/15376516.2015.1053647.

Batra, V., Gopalakrishnan, V., McNeill, J., Hickie, R., 1994. Angiotensin II elevates cytosolic free calcium in human lung adenocarcinoma cells via activation of AT_1 receptors. Cancer Lett. 76, 19–24.

Beyersmann, D., Haase, H., 2001. Functions of zinc in signaling, proliferation and differentiation of mammalian cells. Biometals 14, 331–341.

Bian, F., Cui, J., Zheng, T., Jin, S., 2017. Reactive oxygen species mediate angiotensin II-induced transcytosis of low-density lipoprotein across endothelial cells. Int. J. Mol. Med. 39, 629–635. http://dx.doi.org/10.3892/ijmm.2017.2887.

Biswas, S.K., Rahma, I., 2009. Environmental toxicity, redox signaling and lung inflammation: the role of glutathione. Mol. Asp. Med. 30, 60–76.

Boatright, K.M., Salvesen, G.S., 2003. Mechanisms of caspase activation. Curr. Opin. Cell Biol. 15, 725–731. http://dx.doi.org/10.1016/j.ceb.2003.10.009.

Bookout, K., McCord, S., McLane, K., 2004. Zinc-based barrier cream for treatment of diaper dermatitis in hospitalized infants. J. Wound Ostomy Continence Nurs. 31, S23.

Bradford, M., 1976. A rapid and sensitive method for the quantitation of microgram quantities of protein utilizing the principle of protein-dye binding. Anal. Biochem. 72, 248–254.

Brenner, C., Cadiou, H., Vieira, H.L., Zamzami, N., Marzo, I., Xie, Z., Leber, B., Andrews, D., Duclohier, H., Reed, J.C., Kroemer, G., 2000. Bcl-2 and Bax regulate the channel activity of the mitochondrial adenine nucleotide translocator. Oncogene 19, 329–336. http://dx.doi.org/10.1038/sj.onc.1203298.

Budihardjo, I., Oliver, H., Lutter, M., Luo, X., Wang, X., 1999. Biochemical pathways of caspase activation during apoptosis. Annu. Rev. Cell Dev. Biol. 15, 269–290. http://dx.doi.org/10.1146/annurev.cellbio.15.1.269.

Carter, D.C., Ho, J.X., 1994. Structure of serum albumin. Adv. Protein Chem. 45, 153–203 (and references therein).

CrysAlisPro, 2009. Oxford Diffraction Ltd., Version 1.171.33.48 (Release 15-09-2009 CrysAlis171.NET).

Davis, W., Ronai, Z., Tew, K., 2000. Cellular thiols and reactive oxygen species in drug-induced apoptosis. J. Pharmacol. Exp. Ther. 296, 1–6.

De Wolfi, F.A., Brett, G.M., 2000. Ligand-binding proteins: their potential for application in systems for controlled delivery and uptake of ligands. Pharmacol. Rev. 52, 207–236.

Deacon, G.B., Phillips, R.J., 1980. Relationships between the carbon-oxygen stretching frequencies of carboxylato complexes and the type of carboxylate coordination. Coord. Chem. Rev. 33, 227–250.

Denning, M.F., Wang, Y., Tibudan, S., Alkan, S., Nickoloff, B.J., Qin, J.Z., 2002. Caspase activation and disruption of mitochondrial membrane potential during UV radiation-induced apoptosis of human keratinocytes requires activation of protein kinase C. Cell Death Differ. 9, 40–52. http://dx.doi.org/10.1038/sj.cdd.4400929.

Ding, H.X., Liu, K.K.C., Sakya, S.M., Flick, A.C., O'Donnell, C.J., 2013. Synthetic approaches to the 2011 new drugs. Bioorg. Med. Chem. 21, 2795–2825.

Escobar, E., Rodriguez-Reyna, T., Arrieta, O., Sotelo, J., 2004. Angiotensin II, cell proliferation and angiogenesis regulator: biologic and therapeutic implications in cancer. Curr. Vasc. Pharmacol. 2, 385–399. http://dx.doi.org/10.2174/1570161043385556.

Etcheverry, S.B., Ferrer, E.G., Naso, L., Barrio, D., Lezama, L., Rojo, T., Williams, P.A.M., 2007. Losartan and its interaction with copper(II). Biological effects. Bioorg. Med. Chem. 15, 6418–6424.

Etcheverry, S.B., Di Virgilio, A.L., Nascimento, O.R., Williams, P.A.M., 2012. Dinuclear copper(II) complexes with valsartan. Synthesis, characterization and cytotoxicity. J. Inorg. Biochem. 107, 25–33.

Farrugia, L.J., 1997. ORTEP-3 for windows - a version of ORTEP-III with a graphical user Interface (GUI). J. Appl. Crystallogr. 30, 565.

Finlay, G.J., Baguley, B.C., 2000. Effects of protein binding on the in vitro activity of antitumour acridine derivatives and related anticancer drugs. Cancer Chemother. Pharmacol. 45, 417–422.

Flammer, A.J., Hermann, F., Wiesli, P., Schwegler, B., Chenevard, R., Hürlimann, D., Sudano, I., Gay, S., Neidhart, M., Riesen, W., Ruschitzka, F., Lüscher, T.F., Noll, G., Lehmann, R., 2007. Effect of losartan, compared with atenolol, on endothelial function and oxidative stress in patients with type 2 diabetes and hypertension. J. Hypertens. 25, 785–791. http://dx.doi.org/10.1097/HJH.0b013e3280287a72.

Frezza, M., Hindo, S., Chen, D., Davenport, A., Schmitt, S., Tomco, D., Dou, Q.P., 2010. Novel metals and metal complexes as platforms for cancer therapy. Curr. Pharm. Des. 16, 1813–1825.

Funao, K., Matsuyama, M., Kawahito, Y., Sano, H., Chargui, J., Touraine, J., Nakatani, T., Yoshimura, R., 2009. Telmisartan as a peroxisome proliferator-activated receptor-γ ligand is a new target in the treatment of human renal cell carcinoma. Mol. Med. Rep. 2, 193–198. http://dx.doi.org/10.3892/mmr_00000083.

Gaberc-Porekar, V., Bele, M., Hribar, G., Maver, U., 2011. Zinc-phosphate nanoparticles with reversibly attached TNF-α analogs: an interesting concept for potential use in active immunotherapy. J. Nanopart. Res. 13, 3019–3032.

Ge, Y., Li, T., Cheng, J., 2016. Crystal type I of azilsartan polymorphs: preparation and analysis. J. Cryst. Proc. Technol. 6, 1–10.

Gibellini, L., Pinti, M., Nasi, M., De Biasi, S., Roat, E., Bertoncelli, L., Cossarizza, A., 2012. Interfering with ROS metabolism in cancer cells: the potential role of quercetin. Cancer 2, 1288–1311.

Glaysher, S., Cree, I., 2011. Isolation and culture of colon cancer cells and cell lines. Methods Mol. Biol. 731, 135–140.

Godugu, C., Patel, A.R., Doddapaneni, R., Marepally, S., Jackson, T., Singh, M., 2013. Inhalation delivery of telmisartan enhances Intratumoral distribution of nanoparticles in lung cancer models. J. Control. Release 172, 86–95. http://dx.doi.org/10.

1016/j.jconrel.2013.06.036.
Goldfarb, D., Diz, D., Tubbs, R., Ferrario, C., Novick, A., 1994. Angiotensin II receptor subtypes in the human renal cortex and renal cell carcinoma. J. Urol. 151, 208–213.
Goodsell, D.S., 2002. The molecular perspective: Bcl-2 and apoptosis. Stem Cells 20, 355–356.
He, X.M., Carter, D.C., 1992. Atomic structure and chemistry of human serum albumin. Nature 358, 209–215.
Hemming, K., 2008. In: Katritzky, A.R., Ramsden, C.A., Scriven, E.F.V., Taylor, R.J.K. (Eds.), Comprehensive Heterocyclic Chemistry III. Vol. 5. Elsevier, pp. 243–314.
Hissin, P.J., Hilf, R., 1976. A fluorometric method for determination of oxidized and reduced glutathione in tissues. Anal. Biochem. 74, 214–226.
Ho, E., 2004. Zinc deficiency, DNA damage and cancer risk. J. Nutr. Biochem. 15, 572–578.
Indran, I.R., Tufo, G., Pervaiz, S., Brenner, C., 2011. Recent advances in apoptosis, mitochondria and drug resistance in cancer cells. Biochim. Biophys. Acta - Bioenerg. 1807, 735–745. http://dx.doi.org/10.1016/j.bbabio.2011.03.010.
Islas, M.S., Franca, C.A., Etcheverry, S.B., Ferrer, E.G., Williams, P.A.M., 2012. Computational study and spectroscopic investigations of antihypertensive drugs. Vib. Spectrosc. 62, 143–151.
Islas, M.S., Rojo, T., Lezama, L., Griera Merino, M., Cortes, M.A., Rodriguez Puyol, M., Ferrer, E.G., Williams, P.A.M., 2013. Improvement of the antihypertensive capacity of candesartan and trityl candesartan by their SOD mimetic copper(II) complexes. J. Inorg. Biochem. 123, 23–33.
Islas, M.S., Martínez Medina, J.J., López Tévez, L.L., Lezama, L., Griera Merino, M., Calleros, L., Cortes, M.A., Rodríguez Puyol, M.R., Echeverría, G.A., Piro, O.E., Ferrer, E.G., Williams, P.A.M., 2014. Antitumoral, antihypertensive, antimicrobial and antioxidant effects of an octanuclear copper(II)-telmisartan complex with an hydrophobic nanometer hole. Inorg. Chem. 53, 5724–5737.
Islas, M.S., Luengo, A., Franca, C.A., Griera Merino, M., Calleros, L., Rodriguez-Puyol, M., Lezama, L., Ferrer, E.G., Williams, P.A.M., 2016. Experimental and DFT characterization, antioxidant and anticancer activities of a Cu(II)-irbesartan complex. Structure-antihypertensive activity relationships in Cu(II)-sartan complexes. J. Biol. Inorg. Chem. 21, 851–863.
Jurowski, K., Szewczyk, B., Nowak, G., Piekoszewski, W., 2014. Biological consequences of zinc deficiency in the pathomechanisms of selected diseases. J. Biol. Inorg. Chem. 19, 1069–1079.
Khaper, N., Singal, P., 2001. Modulation of oxidative stress by a selective inhibition of angiotensin II type 1 receptors in MI rats. J. Am. Coll. Cardiol. 37, 1461–1466. http://dx.doi.org/10.1016/S0735-1097(01)01126-3.
Konidaris, K., Gioulib, M., Raptopoulou, C., Psycharis, V., Verginadisb, I., Vasiliadis, A., Afendra, A., Karkabounasb, S., Manessi-Zoupaa, E., Stamatatosa, T., 2013. Employment of pyridyl oximes and dioximes in zinc(II) chemistry: synthesis, structural and spectroscopic characterization, and biological evaluation. Inorg. Chim. Acta 396, 49–59. http://dx.doi.org/10.1016/j.ica.2012.09.039.
Kragh-Hansen, U., 1981. Molecular aspects of ligand binding to serum albumin. Pharmacol. Rev. 33, 17–53.
Kragh-Hansen, U., Chuang, V.T.G., Otagiri, M., 2002. Practical aspects of the ligand-binding and enzymatic properties of human serum albumin. Biol. Pharm. Bull. 25, 695–704 (and references therein).
Kratz, F., Elsadek, B., 2012. Clinical impact of serum proteins on drug delivery. J. Control. Release 161, 429–445.
Kryscko, D.V., Vanden Berghe, T., Parthoens, E., D'Herde, K., Vandenabeele, P., 2008. Methods for distinguishing apoptotic from necrotic cells and measuring their clearance. Methods Enzymol. 442, 307–341. http://dx.doi.org/10.1016/S0076-6879(08)01416-X.
Lagadic-Gossmann, D., Huc, L., Lecureur, V., 2004. Alterations of intracellular pH homeostasis in apoptosis: origins and roles. Cell Death Differ. 11, 953–961.
Lakowicz, J.R. (Ed.), 2013. Principles of Fluorescence Spectroscopy. Springer Science & Business Media, New York.
Lessene, G., Czabotar, P.E., Colman, P.M., 2008. BCL-2 family antagonists for cancer therapy. Nat. Rev. Drug Discov. 7, 989–1000. http://dx.doi.org/10.1038/nrd2658.
Li, X., Rayford, H., Uhal, B.D., 2003. Essential roles for angiotensin receptor AT1a in bleomycin-induced apoptosis and lung fibrosis in mice. Am. J. Pathol. 163, 2523–2530. http://dx.doi.org/10.1016/S0002-9440(10)63607-3.
Ling, L., Tan, K., Lin, H., Chiu, G., 2011. The role of reactive oxygen species and autophagy in safingol-induced cell death. Cell Death Dis. 2, e129.
Lu, S.C., 2013. Glutathione synthesis. Biochim. Biophys. Acta 1830, 3143–3153.
Mamoru, F., Izumi, H., Shohei, Y., Moritoshi, I., Masataka, M., 2002. Blockade of angiotensin AT1a receptor signaling reduces tumor growth, angiogenesis, and metastasis. Biochem. Biophys. Res. Commun. 294, 441–447. http://dx.doi.org/10.1016/S0006-291X(02)00496-5.
Martin, D., Leonardo, M., 1998. Microscopic quantitation of apoptotic index and cell viability using vital and fluorescent dyes. Curr. Protoc. Immunol. 1, 3.17.1–3.17.39.
Maryam, A., Mehmood, T., Zhang, H., Li, Y., Khan, M., Ma, T., 2017. Alantolactone induces apoptosis, promotes STAT3 glutathionylation and enhances chemosensitivity of A549 lung adenocarcinoma cells to doxorubicin via oxidative stress. Sci. Report. 7 (6242), 1–18. http://dx.doi.org/10.1038/s41598-017-06535-y.
Masuoka, J., Hegenauer, J., Van Dyke, B.R., Saltman, P., 1993. Intrinsic stoichiometric equilibrium constants for the binding of zinc(II) and copper(II) to the high affinity site of serum albumin. J. Biochem. Mol. Biol. 268, 21533–21587.
Moneo Ocaña, V., Santamaría Núñez, G., García Fernández, L.F., Galmarini, C.M., Guillén Navarro, M.J., Avilés Marín, P.M., 2012. Combination Therapy With an Antitumor Alkaloid. International Application No. PCT/EP2011/069976. Pub. No.: WO/2012/062920.
Ndagi, U., Mhlongo, N., Soliman, M.E., 2017. Metal complexes in cancer therapy - an update from drug design perspective. Drug Des. Devel. Ther. 11, 599–616. http://dx.doi.org/10.2147/DDDT.S119488.
Oh, E., Kim, J., Cho, Y., An, H., Lee, N., Jo, H., Ban, C., Seo, J., 2015. Overexpression of angiotensin II type 1 receptor induces epithelial-mesenchymal transition and promotes tumorigenesis of human breast cancer cells. Cancer Res. 75 (15) (Abstract 1445). https://doi.org/10.1158/1538-7445.AM2015-1445.
Okada, M., Suzuki, K., Matsumoto, M., Takada, K., Nakanishi, T., Horikoshi, H., Higuchi, T., Hosono, Y., Nakayama, M., Ohsuzu, F., 2009. Effects of angiotensin on the expression of fibrosis-associated cytokines, growth factors, and matrix proteins in human lung fibroblasts. J. Clin. Pharm. Ther. 34, 289–299. http://dx.doi.org/10.1111/j.1365-2710.2008.01006.x.
Pendergrassa, K., Gwathmey, T., Michalek, R., Grayson, J., Chappella, M., 2009. The angiotensin II–AT1 receptor stimulates reactive oxygen species within the cell nucleus. Biochem. Biophys. Res. Commun. 384, 149–154. http://dx.doi.org/10.1016/j.bbrc.2009.04.126.
Pialoux, V., Foster, G.E., Ahmed, S.B., Beaudin, A.E., Hanly, P.J., Poulin, M.J., 2011. Losartan abolishes oxidative stress induced by intermittent hypoxia in humans. J. Physiol. 589, 5529–5537. http://dx.doi.org/10.1113/jphysiol.2011.218156.
Piastowska-Ciesielska, A., Domińska, K., Nowakowska, M., Gajewska, M., Gajos-Michniewicz, A., Ochędalski, T., 2014. Angiotensin modulates human mammary epithelial cell motility. J. Renin-Angiotensin-Aldosterone Syst. 15, 419–429. http://dx.doi.org/10.1177/1470320313475904.
Plotnikova, O.A., Melnikov, G.V., Melnikov, A.G., Kovalenko, A.V., 2016. Comparative studies of the effects of copper sulfate and zinc sulfate on serum albumins. Proc. SPIE 9917 (99170Z1–99170Z7).
Podowski, M., Calvi, C., Metzger, S., Misono, K., Poonyagariyagorn, H., Lopez-Mercado, A., Neptune, E., 2012. Angiotensin receptor blockade attenuates cigarette smoke–induced lung injury and rescues lung architecture in mice. J. Clin. Invest. 122, 229–240. http://dx.doi.org/10.1172/JCI46215.
Ross, P.A., Subramunian, S., 1981. Thermodynamics of protein association reactions: forces contributing to stability. Biochemistry 20, 3096–3102.
Säbel, C.E., Neureuther, J.M., Siemann, S., 2010. A spectrophotometric method for the determination of zinc, copper, and cobalt ions in metalloproteins using Zincon. Anal. Biochem. 397, 218–226.
Sharma, S., Venkatesan, V., Prakhya, B.M., Bhonde, R., 2015. Human mesenchymal stem cells as a novel platform for simultaneous evaluation of cytotoxicity and genotoxicity of pharmaceuticals. Mutagenesis 30, 391–399. http://dx.doi.org/10.1093/mutage/geu086.
Sheldrick, G.M., 2008. A short history of *SHELX*. Acta Crystallogr. A64, 112–122.
Šikić Pogačar, M., Maver, U., Marčun Varda, N., Mičetić-Turk, D., 2017. Diagnosis and management of diaper dermatitis in infants with emphasis on skin microbiota in the diaper area. Int. J. Dermatol. http://dx.doi.org/10.1111/ijd.13748.
Szatrowski, T.P., Nathan, C.F., 1991. Production of large amounts of hydrogen peroxide by human tumor cells. Cancer Res. 51, 794–798.
Tamura, K., Ohsawa, M., Kanaoka, T., Maeda, A., Azushima, K., Uneda, K., Wakui, H., Azuma, K., Tsurumi-Ikeya, Y., Umemura, S., 2013. What can we expect from the binding characteristics of azilsartan, a newly available angiotensin II blocker, in hypertension? Hypertens. Res. 36, 107–108.
Toyokuni, S., Okamoto, K., Yodoi, J., Hiai, H., 1995. Persistent oxidative stress in cancer. FEBS Lett. 358, 1–3.
Truong-Tran, A., Carter, J., Ruffin, R., Zalewski, P., 2000. New insights into the role of zinc in the respiratory epithelium. Immunol. Cell Biol. 79, 170–177. http://dx.doi.org/10.1046/j.1440-1711.2001.00986.x.
Uhal, B.D., Wang, R., Laukka, J., Zhuang, J., Soledad-Conrad, V., Filippatos, G., 2003. Inhibition of amiodarone-induced lung fibrosis but not alveolitis by angiotensin system antagonists. Pharmacol. Toxicol. 92, 81–87. http://dx.doi.org/10.1034/j.1600-0773.2003.920204.x.
Vyssokikh, M.Y., Zorova, L., Zorov, D., Heimlich, G., Jürgensmeier, J.J., Brdiczka, D., 2002. Bax releases cytochrome c preferentially from a complex between porin and adenine nucleotide translocator. Hexokinase activity suppresses this effect. Mol. Biol. Rep. 29, 93–96. http://dx.doi.org/10.1023/A:1020383108620.
Wang, R., Zagariya, A., Ibarra-Sunga, O., Gidea, C., Ang, E., Deshmukh, S., Chaudhary, G., Baraboutis, J., Filippatos, G., Uhal, B., 1999. Angiotensin II induces apoptosis in human and rat alveolar epithelial cells. Am. J. Phys. Lung Cell. Mol. Phys. 276, 885–889.
Weidner, N., Semple, J.P., Welch, W.R., Folkman, J., 1991. Tumor angiogenesis and metastasis—correlation in invasive breast carcinoma. N. Engl. J. Med. 324, 1–8. http://dx.doi.org/10.1056/NEJM199101033240101.
Williams, P.A.M., 2013. Metal complexes of the antihypertensive drugs that inhibit the renin-angiotensin system. Curr. Trends Med. Chem. 7, 97–104.
Yuan, N., Wang, Y., Li, K., Zhao, Y., Hu, X., Mao, L., Zhao, W., Lian, H., Zheng, W., 2012. Effects of exogenous zinc on the cellular zinc distribution and cell cycle of A549 cells. Biosci. Biotechnol. Biochem. 76, 2014–2020.
Zaiken, K., Cheng, J.W., 2011. Azilsartan medoxomil: a new angiotensin receptor blocker. Clin. Ther. 33, 1577–1589.
Zhang, Y., Shi, S., Sun, X., Xiong, X., Peng, M., 2011. The effect of Cu^{2+} on interaction between flavonoids with different C-ring substituents and bovine serum albumin: structure-affinity relationship aspect. J. Inorg. Biochem. 105, 1529–1537.
Zhang, L., Cai, Q.Y., Cai, Z.X., Fang, Yi, Zheng, C.S., Wang, L.L., Lin, S., Chen, D.X., Peng, J., 2016. Interactions of bovine serum albumin with anti-cancer compounds using a ProteOn XPR36 Array biosensor and molecular docking. Molecules 21, 1706. http://dx.doi.org/10.3390/molecules21121706.
Zhao, W., Song, Q., Zhang, Z., Mao, L., Zheng, W., Hu, X., Lian, H., 2015. The kinetic response of the proteome in A549 cells exposed to $ZnSO_4$ stress. PLoS One 10, e0133451.
Ziegler, U., Groscurth, P., 2004. Morphological features of cell death. Physiology 19, 124–128. http://dx.doi.org/10.1152/nips.01519.2004.